
**Università degli Studi di Torino**

Dipartimento di Fisica
Scuola di Scienze della Natura

# Modeling and simulation of sputter-ion pump performances

**Candidato:**
**Tiziano Isoardi**

**Relatore:**
**Prof. Alessandro Ferretti**

**A.A. 2021/2022**

# Contents

# Chapter 1

# Introduction

Vacuum studies have always contributed to scientific and technological evolution. Situations of absolute vacuum have never been observed in nature nor obtained in laboratory, however different degrees of vacuum can be defined, depending on the pressure range considered. This thesis will be about systems that work at ultra-high vacuum (UHV), condition which is characterized from pressures between $10^{-5}$ and $10^{-10}$ mbar. In this situation the gas molecules are in free molecular flow: their mean free path is of the order of tens of kilometers, i.e. much greater than the dimensions of the system. In this regime the rate of collisions between molecules is negligible with respect to the one with the system walls.

UHV systems are used in different research fields, such as surface science, mass spectroscopy, particle accelerators etc. A way to reach these pressures is to use an ion pump, which comes in three different types: standard diode pump, noble diode pump and triode pump. This thesis will refer to the standard diode pump, in particular the sputter ion pump (SIP) which is a

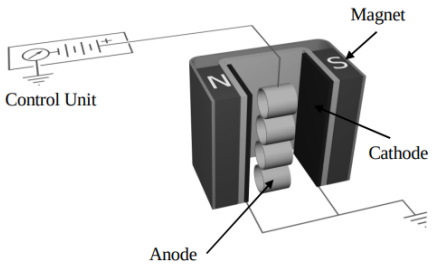


**Figure 1.1:** *Configuration of a sputter ion pump*

vacuum pump that operates by sputtering a metal getter. A typical SIP is composed by arrays of Penning traps with a cylindrical anode placed between two Titanium cathodes and two permanent magnets [42] (see Fig.1.1).

Typical voltages applied at the anode is between 3 kV and 7 kV, while the cathodes are grounded. The magnetic field has a magnitude of about 0.1 T and its direction is parallel to the axis of the cylindrical anode. The resulting electromagnetic field is able to trap moving electrons inside the cylindrical space, making them to oscillate around the trap center along the trap axis direction.

The operation of the pump starts thanks to electrons freed inside the system by cathode emission or by cosmic rays. Trapped electrons collide with molecules of residual gases (typically $H_2$, CO, $CO_2$, $N_2$, $H_2O$, Ar, He) ionizing them. The EM field accelerates positively ionized molecules toward cathodes. The ion-cathode collisions generate sputtering phenomena of chemically active Titanium film on anode: neutral getterable gas molecules attach to Titanium film and captured by the anode (see Fig.1.2) [3]. Moreover, ion-cathode collisions induce free electrons emission from cathode that feed the gas ionization process.

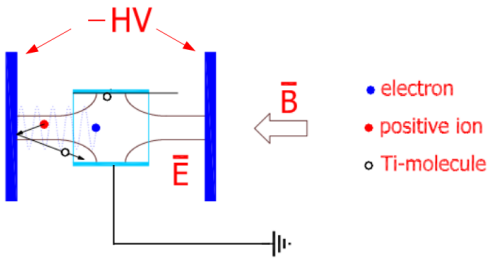


**Figure 1.2:** *The Penning cell and the configuration of the electric and magnetic field that trap the electrons and remove the ions. The ion-cathode collisions sputter the Titanium molecules*

Since electrons emitted from the cathode have sufficient energy to ionize more than once, it could naively be expected to have an exponential increase of the current until the complete emptying of gas molecules. On the contrary, the current stabilizes almost immediately.

Since the gas emptying speed is proportional to the current value, studying the causes of current saturation is crucial to improve the performance of the ion pump. Since the amplitude of the electrons oscillation along the trap axis depends on their kinetic energy, the electrons kinetic energy loss (after the ionizations) reduces the amplitude of their oscillations to a small region around the trap center. The electrons concentrated in this volume do not contribute to the ionization of gas molecules (because of their low kinetic energy) but they generate a non negligible space charge effect which could lead to current saturation.

This thesis work originated from a collaboration between Università degli Studi di Torino and Agilent Technologies Italia S.p.A. and its aim is to study and implement an efficient physics-based numerical model able to describe the operation of the Agilent sputter ion pumps, taking into account all the main parameters that influence their action. The challenge is to identify the

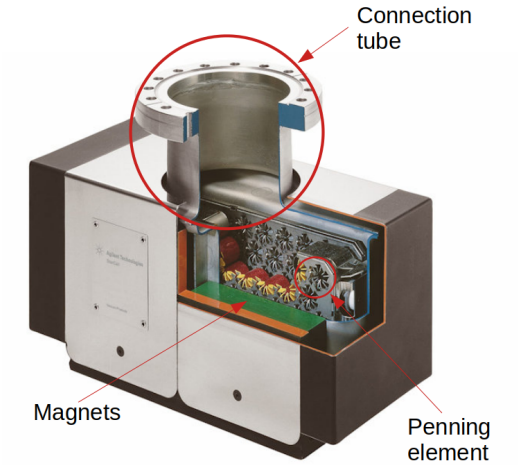


**Figure 1.3:** *An example of an ion Agilent's diode VIP ion pump*

main phenomena occurring inside the pump and simulate them, balancing consistency with reality and simulation time. It will be seen in the next chapters that the efficiency of a pump depends mainly on the number of electrons trapped in it. Since number of electrons in a single Penning cell is of the order of $10^{10}$ - $10^{11}$, the algorithm has to describe the behavior of these electrons in a reasonable time.

# Chapter 2

# The Penning trap

The Penning trap [9] is the fundamental component of a sputter ion pump. It is a device which confines free charged particles using a quadrupolar electric field combined with a dipolar magnetic field parallel at the axis of the trap. The fields have the form:

$$\vec{E}(x,y,z) = \frac{U_0}{2d^2}(x\hat{e}_x + y\hat{e}_y - 2z\hat{e}_z) \tag{2.1}$$

$$\vec{B} = B_0\hat{e}_z \tag{2.2}$$

where $U_0$ is the cathodes voltage and $d=\sqrt{(z_0^2 + \rho_0^2/2)/2}$ is the so called trap dimension: $2z_0$ is the distance between cathodes and $\rho_0$ is the radius of the anode (see Fig.2.1). The electric field traps electrons along the axial direction while the magnetic field traps them radially [12]. The motion of a free charge inside the Penning cell without background gas can be obtained from the Lorentz force:

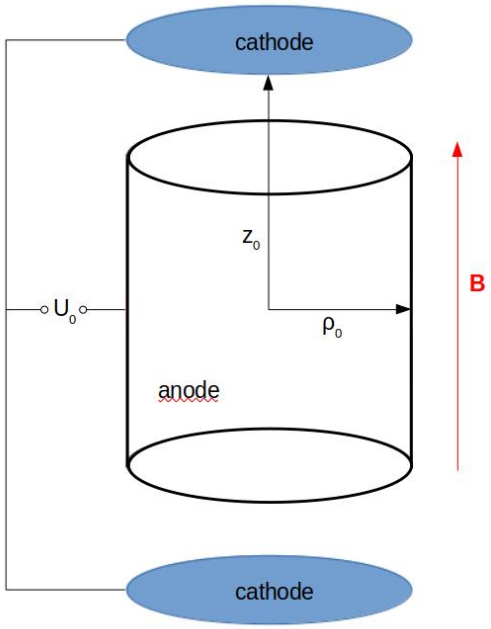


**Figure 2.1:** *The Penning trap*

$$\vec{F} = m\ddot{\vec{r}} = q(\vec{E} + \dot{\vec{r}} \times \vec{B}) \tag{2.3}$$

Given the equations of the electric and magnetic field (Eq.2.1 and Eq.2.2), the equations of motion for a single particle are:

$$\begin{aligned} \ddot{x} + \omega_c \dot{y} - \frac{\omega_z^2}{2} x = 0 \\ \ddot{y} - \omega_c \dot{x} - \frac{\omega_z^2}{2} y = 0 \\ \ddot{z} + \omega_z^2 z = 0 \end{aligned} \tag{2.4}$$

where:

$$\begin{aligned} \omega_c = \frac{qB}{m} \\ \omega_z = \sqrt{\frac{qU_0}{md^2}} \end{aligned} \tag{2.5}$$

So the axial motion of a single charge is an harmonic oscillation with a frequency $\omega_z$ which is decoupled from the motion on the radial plane. The description of the radial motion can be expressed considering the complex variable:

$$u = x + iy \tag{2.6}$$

In this way the motions along $x - y$ axes can be expressed by the single equation:

$$\ddot{u} + i\omega_c\dot{u} - \frac{1}{2}\omega_z^2 u = 0 \tag{2.7}$$

The solution of this equation can be found by setting $u = exp(-i\omega t)$ yielding the condition:

$$\omega^2 - \omega_c\omega + \frac{1}{2}\omega_z^2 = 0 \tag{2.8}$$

which has two solutions $\omega_+$ and $\omega_-$:

$$\begin{aligned} \omega_+ &= \frac{1}{2}\left[\omega_c + \sqrt{\omega_c^2 - 2\omega_z^2}\right] \\ \omega_- &= \frac{1}{2}\left[\omega_c - \sqrt{\omega_c^2 - 2\omega_z^2}\right] \end{aligned} \tag{2.9}$$

So the total motion of a single charge in a Penning trap can be decoupled in three independent motions with a specific oscillation frequency:

- the axial oscillation $\omega_z$: is a movement parallel to the axis of the trap and is caused by the presence of the electric field (see Eq.2.5);
- the cyclotron motion $\omega_+$: is a fast rotation on the radial plane due to the magnetic field.

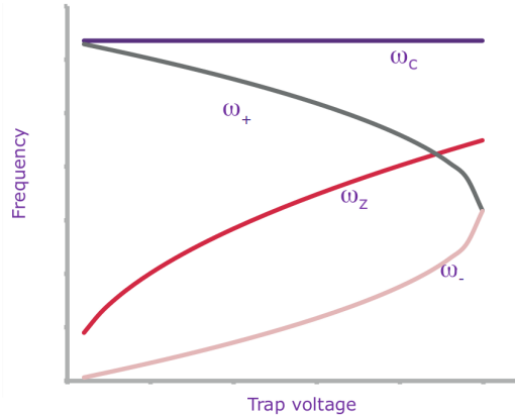


**Figure 2.2:** *The oscillation frequencies related to the supply voltage*

- the magnetron motion $\omega_-$: is a slow rotation on the radial plane around the axis and is caused by both the electric and the magnetic fields. This causes a drift of the particle in a plane perpendicular to the magnetic field.

The magnetron motion could be less intuitive to understand than the other two. A physical interpretation of this motion can be obtained starting from the equilibrium of the forces acting radially on the electrons:

$$qv_dB = qE_r \rightarrow \omega_d = \frac{v_d}{r} = \frac{E_r}{Br} \tag{2.10}$$

The centrifugal force caused by the radial electric field can be balanced by an opposite force if the tangential speed (the drift velocity $v_d$) is different from zero [7]. This speed is linked with the operating and geometrical parameters as:

$$v_d = \frac{U_0 r}{2Bd^2} \rightarrow \omega_d = \frac{U_0}{2Bd^2} \tag{2.11}$$

In this thesis the region of interest of Penning traps is at low voltages where

the relationships between frequencies are (see Fig.2.2):

$$\begin{aligned} \omega_c &= \omega_+ + \omega_- \\ \omega_+ &\gg \omega_z \gg \omega_- \end{aligned} \tag{2.12}$$

In a first approximation the magnetron and cyclotron frequencies can be calculated as:

$$\begin{aligned} \omega_- &\simeq \frac{U_0}{2Bd^2} \\ \omega_+ &\simeq \omega_c = \frac{qB}{m} \end{aligned} \tag{2.13}$$

From Eq.2.11 and Eq.2.13 it is clear that the magnetron oscillation is caused by the drift of the electrons on the radial plane. The trap becomes unstable when $\omega_c^2 < 2\omega_z^2$. In this case the radial force that pushes the charge through the anode is able to overcome the magnetic confinement. As shown on Fig.2.2 all these frequencies depend from the trap voltage, so it is possible to express the stable confinement as a relation between applied fields, in order to obtain the minimum magnetic field which confines radially the electrons [50]:

$$\frac{qB^2}{m} > \frac{2U_0}{d^2} \tag{2.14}$$

Considering a Penning trap with a radius of about 10 mm, an height of about 25 mm, a cathode voltage of -3 kV and a magnetic field of 0.1 T the cyclotron frequency is of the order of 10 GHz, the axial frequency is of the order of 1 GHz and the magnetron frequency is of the order of 0.01 GHz. So, the typical work conditions of a SIP are within the Penning trap stability regime. In Fig.2.3 a completely trapped particle trajectory in an ideal Penning trap is shown.

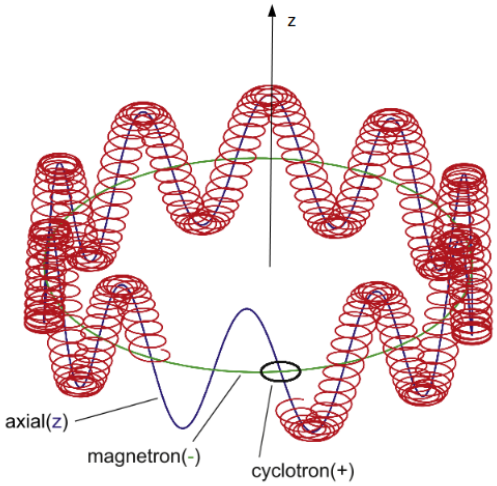


**Figure 2.3:** *Trajectory of the trapped particle inside the trap [12]*

## 2.1 Electron energy in a Penning trap

In every point of the electron trajectory in the trap it is possible to calculate the total energy of the electron. This is the sum of the potential and kinetic energy associated to each of the three independent oscillations.

### 2.1.1 Axial oscillation

The energy associated to the axial oscillation is given by this equation:

$$E = \frac{1}{2}[mz^2\omega_z^2 + mv_z^2] = \frac{1}{2}mz_0^2\omega_z^2 \tag{2.15}$$

where $z_0$ is the amplitude of the axial oscillation. It is important to notice that the total energy is proportional to the oscillation amplitude.

### 2.1.2 Cyclotron oscillation

The energy associated to the cyclotron oscillation is given by this equation:

$$E = -\frac{1}{4}mr_c^2\omega_z^2 + \frac{1}{2}mv_c^2 = \frac{1}{2}mr_c^2\omega_+(\omega_+ - \omega_-) \tag{2.16}$$

where $r_c$ is the cyclotron radius

### 2.1.3 Magnetron oscillation

The energy associated to the magnetron oscillation is given by this equation:

$$E = -\frac{1}{4}mr_m^2\omega_z^2 + \frac{1}{2}mv_m^2 = -\frac{1}{2}mr_m^2\omega_-(\omega_+ - \omega_-) \tag{2.17}$$

where $r_m$ is the magnetron radius

The total magnetron energy is negative, so a loss of electron energy leads to an increase of its magnetron radius and a decrease of oscillation amplitude on the axis [51].

## 2.2 Collisions with background gas

In the previous section the motion of a single charge in an empty trap was described, together with the distribution of energy along its trajectory. The next step is to consider the presence of a certain background gas and to calculate what happens to the electron trajectories.

It is well known that when an electron interacts with a gas particle, three different type of collision can arise: elastic, non-ionizing inelastic and ionization. These probabilities are described by cross-sections which depend

by the electron energy and by the background molecule. After the collision, the electron changes its trajectory and velocity and can lose a part of its energy. In this last case, referring to Eq.2.15, Eq.2.16, Eq.2.17, the electron reduces its oscillation amplitude along the axis, reduce its cyclotron radius and increase its magnetron radius. In Fig.2.4 is reported an example of an electron radial trajectory which is losing energy at a constant rate.

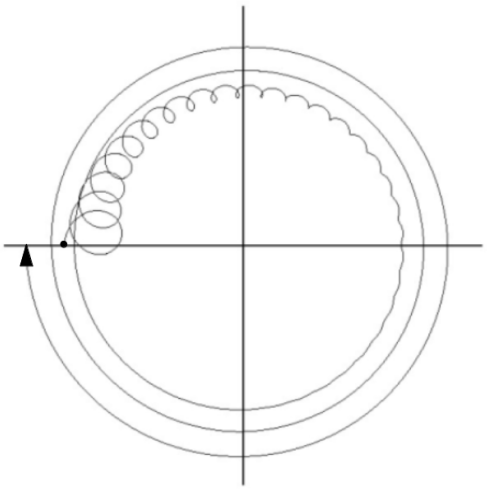

**Figure 2.4:** *Trajectory in the radial plane of a single electron which is losing energy. Initially the electron has a certain energy correlated to the cyclotron and magnetron radius. Losing energy, its magnetron radius increases while its cyclotron radius shrinks*

After a certain number of inelastic collisions the electrons oscillation along the axis becomes small, leading to an accumulation of charges in a restricted volume: in this case the space charge effect is not negligible and plasma effects will have to be considered.

Obviously, the actual change in trajectory is not like the one in the example figure: the energy loss is not continuous but discrete. Moreover the real trajectory is subjected to the statistical fluctuation of the direction after the

collisions. Therefore, after a collision, the direction of the electron can be random, as long as the conservation of total energy is respected.
This means that, in real life, it is not always true that, after a collision, the oscillation along the axis reduces its amplitude and the magnetron radius increases. After a collision, an electron could, for example, increases its axial oscillation (with an increase in energy) provided that its radial oscillation is modified in order to conserve the total energy. So the "ideal" behaviors are true only statistically, considering a time much greater than the average time between two consecutive collisions, as it will be shown in the following.

## 2.3 Electron plasma

As explained in the previous section, after a certain number of collisions the electrons lose most of their energy and remain confined in a small region of the trap. The increase of the number of electrons in this region leads to the formation of a non-neutral plasma of electrons. This is a plasma with a single sign of charge which can be in principle confined forever using electrostatic and magnetic field. This type of plasma can be in a state of thermal equilibrium, allowing to describe it with a thermodynamics approach [11].
In order to treat an electron cloud as a plasma, its dimensions must be larger than the Debye length $\lambda_D$ defined as:

$$\lambda_D = \sqrt{\frac{\epsilon_0 kT}{nq^2}} \tag{2.18}$$

where *T* is the temperature of the electrons, *k* is the Boltzmann constant, *q* the single electron charge and *n* is the plasma density. The temperature of the plasma electrons in the trap is of the order of $10^5$ K: this value is calculated assuming that their energy is not sufficient to ionize further molecules. Considering an average ionization energy of about 15 eV it is possible to calculate the order of magnitude of their temperature.

For what concerns the calculation of plasma density *n* in a system with cylindrical symmetry, it has to satisfy the Poisson equation:

$$\nabla\Phi(r,z) = -\frac{n(r,z)}{\epsilon_0} \tag{2.19}$$

The density has the form:

$$n(r,z) = n_0 exp\{-[q\Phi(r,z) + \frac{1}{2}m\omega(\omega_c - \omega)r^2]/(kT)\} \tag{2.20}$$

The thermal equilibrium condition is satisfied by the Gibbs distribution [28] which can be written as:

$$f(\vec{s},\vec{v}) = n(r,z)(\frac{m}{2\pi kT})^{\frac{3}{2}} exp(-\frac{1}{2}m\frac{(\vec{v}+\omega r\hat{\theta})^2}{kT}) \tag{2.21}$$

This is the Maxwell-Boltzmann distribution in a frame rotating with a frequency $\omega$. In this system the plasma electrons are free. From Eq.2.20 it is possible to distinguish three different potential: the electric potential $\Phi(r,z)$, the centrifugal potential -$m\omega^2r^2/2$ and the potential that allows the radial confinement $m\omega\omega_c r^2/2$. These potentials depend on the sign of the charge, so a confinement of the electrons means a non-confinement of the ions [35]. Considering the limit of temperature T→0, the only way to obtain

a non-divergent density is to consider:

$$q\Phi(r,z) + \frac{1}{2}m\omega(\omega_c - \omega)r^2 = 0 \tag{2.22}$$

From this last condition and from the solution of the Poisson equation, the constant density inside the plasma is obtained as:

$$n = \frac{2m\epsilon_0}{q}\omega(\omega_c - \omega) = \frac{m\epsilon_0}{q}\omega_p^2 \tag{2.23}$$

where $\omega_p$ is the plasma frequency [11] and it is calculated as:

$$\omega_p = \sqrt{\frac{q^2 n}{\epsilon_0 m}} \tag{2.24}$$

The maximum density that can be reached inside the plasma is given by the *Brillouin limit*:

$$n_B = \frac{B^2}{2\mu_0 m c^2} \tag{2.25}$$

Assuming a long confinement time ($t$>>1 ms) and thermal equilibrium the electrons cloud density can be considered uniform. When the plasma has reached the Brillouin limit the value of $\omega_p$ is equal to $\omega_c/\sqrt{2}$ (see Fig.2.5). All these calculations are done starting from the hypothesis of T→0. From [38] is demonstrated that for non-zero temperatures the plasma density is constant up to the edge of plasma and go to zero in a Debye length (see Fig.2.6).

Another more intuitive way to calculate the electron density inside the plasma and to find out the Brillouin limit is by considering the sum of forces acting on

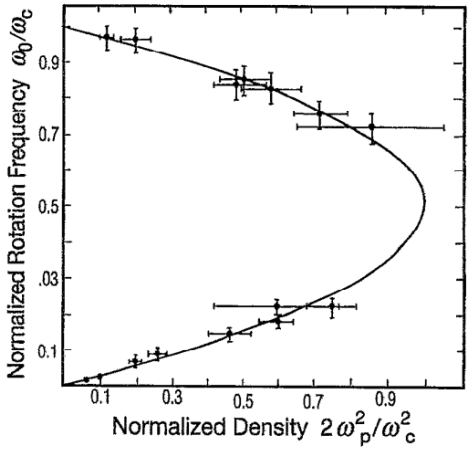


**Figure 2.5:** *The variation of the plasma frequency with respect to the cyclotron one. When the condition $2\omega_p^2=\omega_c^2$ is reached the plasma is in the Brillouin limit [13]*

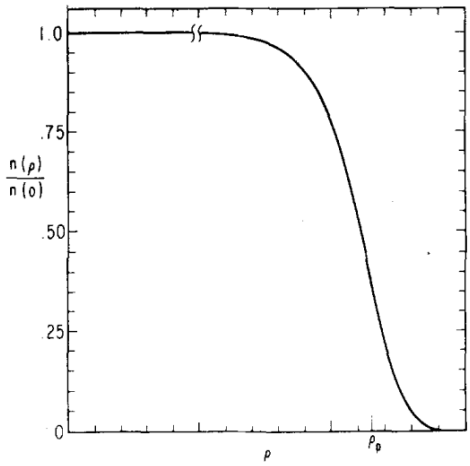


**Figure 2.6:** *The density inside a plasma is constant until to the edge of plasma and go to zero in around a Debye length*

the plasma. In this case, the Coulomb repulsive force induces a rotary motion in the plasma that balances the outward forces caused by the non-neutral plasma and centrifugal force [5]. All the radial forces are balanced when the following condition is met:

$$qE_{\mathrm{r}} + qv_\theta B + \frac{m{v_\theta}^2}{r} = 0 \tag{2.26}$$

where $E_r$ is the radial component of the electric field, $m$ is the electron mass, $B$ is the magnitude of magnetic field and $v_\theta$ is the rotational velocity. Solving the equation for $v_\theta$ and considering that the rate of rotation is $\omega$ = -$v_\theta$/r the result is:

$$\omega \simeq \frac{\omega_{\mathrm{c}}}{2} \pm \sqrt{\frac{{\omega_{\mathrm{c}}}^2}{4} - \frac{qE_{\mathrm{r}}}{mr}} \tag{2.27}$$

The two rotation modes meet when $qE_r/mr={\omega_c}^2/4$. In this case the Brillouin limit represents the maximum radial electric field that allows plasma confinement. Using the Poisson equation it is possible to find the relation between the radial electric field and the plasma density $n$:

$$\frac{1}{r} \cdot \frac{\partial}{\partial r}(rE_{\mathrm{r}}) \simeq \frac{qn}{\epsilon_0} \tag{2.28}$$

Solving this equation the maximum density of the plasma is:

$$n \simeq \frac{2\epsilon_0 m\omega(\omega_{\mathrm{c}} - \omega)}{q^2} \tag{2.29}$$

$$\Rightarrow n_{\mathrm{B}} \simeq \frac{\epsilon_0 m{\omega_{\mathrm{c}}}^2}{2q^2} = \frac{B^2/(2\mu_0)}{mc^2} \tag{2.30}$$

Thus, the maximum density in a non-neutral plasma depends from the magnitude of the magnetic field and from the charged particle mass. In our case, i.e. an electron plasma with a magnetic field of 0.1 T, the maximum density is about $10^{10} \frac{electrons}{cm^3}$. Taking into account this value of density and considering a temperature of charges of about $10^5$ K, the reference Debye length is about 0.1 mm.

# Chapter 3

# Pumping mechanisms and performances parameters

There are different quantities which can be measured in a vacuum pump to describe its performances: volumetric flow (pumping speed), mass flow (throughput), compression ratio and pressure difference between discharge and inlet. These values can be linked in order to understand the operation of the pump. The throughput $Q$ describes the volume of gas which crosses a plane in a certain time multiplied by the pressure at the plane [15]:

$$Q = \frac{d(pV)}{dt} = \frac{dn}{dt}RT \tag{3.1}$$

where $n$ is the number of moles, $R$ is the universal gas constant and $T$ is the gas temperature. From Eq.3.1 we can think of $Q$ as the flow of energy per unit of time.

In a steady state the flow does not change in time, so the throughput is constant. Starting from the definition of throughput we can define the

pumping speed *S* as the ratio between the throughput and the inlet pressure *P*:

$$S = \frac{Q}{P} \tag{3.2}$$

*S* represents the volume of gas removed from the system in a certain time (it is expressed in *l/s* or $m^3/s$).

The relation most used to characterize the performances of a pump is the pumping speed *S*. It is not easy to measure *S*, because it depends from different processes such as sputtering, conductance, ion current, etc. which will be explained in this chapter. Two types of pumping speed can be calculated: the *ionization pumping speed S* and the *measured pumping speed* $S_{eff}$, whose maximum value is the *nominal pumping speed* and is given by the manufacturer, which describes the effective amount of gas pumped. The first speed is proportional to the relationship between current and pressure and the second one can be calculated starting from the ionization speed and taking into account other parameters of the pump. *S* is obtained as:

$$S = \frac{V}{t} = \frac{NRT}{tPN_A} = \frac{RT}{qN_A} \cdot \frac{Nq}{tP} = k\frac{I}{P} \tag{3.3}$$

where *I* is the ion current and *k* is a constant. Thus another useful quantity to assess the performance of an ion pump is the relationship between ion current and pressure. The measured pumping speed can be calculated at low pressures as:

$$S_{eff} = (\frac{1}{SC \cdot S'} + \frac{1}{C})^{-1} \tag{3.4}$$

where *SC* is the sticking coefficient, which depends from the degree of coverage of the anode by the Titanium active film as we can see later; *C* is the conductance (expressed in *l/s*) of the connection pipe between the pump and the volume to pumped; *S'* is the ionization pumping speed that takes into account the conductance due to the gap between anode and cathodes (which describes the ease with which the gas passes through this gap) which can be calculated as:

$$S' = S \cdot \frac{tanhD}{D} \tag{3.5}$$

$$D = \frac{ka}{7.85\alpha}\sqrt{\frac{IPS}{ab}} \tag{3.6}$$

where *a* and *b* are respectively the depth and length of pump unit in cm, $\alpha$ is the gap in cm and *k* is a factor equal to 1 if the pumping unit is open to one side and 0.5 for two open sides [14]. In this case *k* will be considered equal to 1. From Eq.3.4 is clear that the measured pumping speed is lower than the ionization one.

## 3.1 Sticking coefficient

One of the parameters needed to calculate the measured pumping speed is the sticking coefficient on Titanium film. It represents the probability of the background gas which interacts with the surface to be absorbed, and is a function of the percentage of Titanium covered area that can be calculated using the Langmuir isotherm model [1]. It depends on the background gas

pressure and on the sputtering yield of metal atoms that regenerate film on anode [20]. The sticking coefficient can be obtained as:

$$SC = SC_0(1-\theta) \tag{3.7}$$

where $SC_0$ is the sticking coefficient at zero coverage and $\theta$ is the percentage of surface coverage. It can be calculated for the monoatomic and diatomic gas respectively as [17, 32]:

$$\theta_{mono} = \frac{KP}{1+KP} \tag{3.8}$$

$$\theta_{di} = \frac{\sqrt{KP}}{1+\sqrt{KP}} \tag{3.9}$$

where $P$ is the gas pressure and $K$ is a constant that depends on the temperature $T$, activation energy $U$, number of sites capable of binding the adsorbate per unit area $N$, area $\sigma_0$, weight of molecule $m$ and absorption time $\tau_0$:

$$K = \frac{k_1}{k_2} \tag{3.10}$$

where:

$$k_1 = \frac{1}{\tau_0} exp(-U/k_B T) \tag{3.11}$$

$$k_2 = \frac{N\sigma_0}{\sqrt{2\pi m k_B T}} \tag{3.12}$$

In this case the total $\theta$ depends on the number of available sites which have not absorbed gas molecules and on the sites that are regenerated from

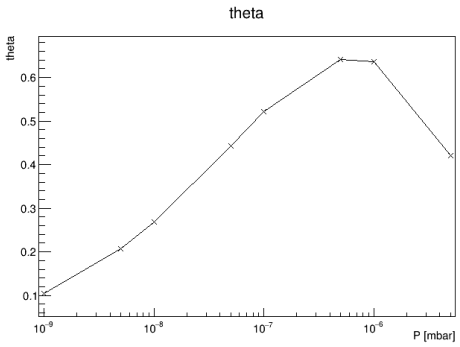


**Figure 3.1:** *Degree of coverage at different pressures of Titanium anode from $N_2$ gas molecules*

sputtered Titanium molecules. Considering this, the degree of coverage of Titanium anode by a certain background gas changes with pressure as shown on Fig.3.1:

## 3.2 Sputtering

Sputtering is the process which allows to extract atoms from a target material following a collision with an energetic ion.

As explained in the previous chapter, the Penning cells in the ion pumps are configured to trap the electrons and to accelerate the ions toward one of the two Titanium cathodes. After the collision with the cathode, the ion can sputter Titanium and electrons. The Titanium atoms can deposit on this anode forming an active absorbing film, while the electrons stay in the trap and continue to ionize molecules; the ion can remain buried inside the cathode. In principle, this ion-burying mechanism removes the residual molecules reducing the pressure. However, the electron discharge produces multiple ionizations leading to a bombardment of the cathode by many ions which can erode it. The erosion of the cathode is not uniform due to the

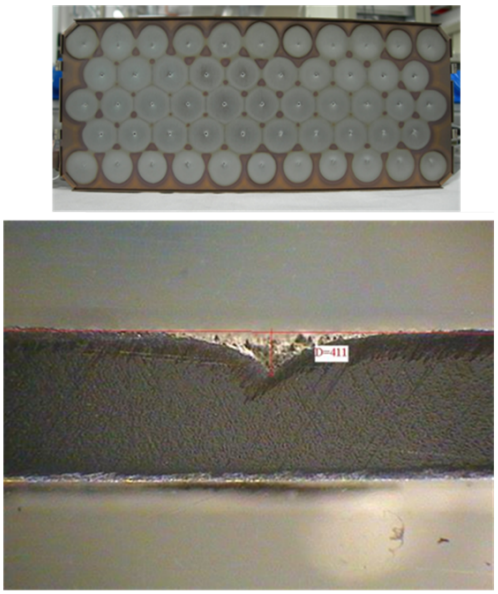

**Figure 3.2:** *The erosion of the cathode in an ion Pump. In the top figure it is possible to distinguish the erosion of the cathode in correspondence of the Penning cells axes. In the bottom image is figured the transverse profile of an eroded cathode*

electromagnetic field configuration which pushes the ions towards the axis of the Penning cell (see Fig.3.2).

Due to erosion, the ions which were previously buried in the cathode can be released back in the cell, increasing the pressure (unstable pumping). When the number of ions implanted in the cathode by collisions and the number of ions released back due to erosion is equal, the pump is in a saturated state [41]. This doesn't mean that the pumping speed go to zero: after the saturation point the pumping speed depends only from the chemisorption of the neutral molecules by the Titanium active film on anode. The time needed to the pump to saturate depends on the starting pressure: lower starting pressures implies longer saturation times (see Fig.3.3)

Sputtered atoms are ejected from the target not because of a direct collision

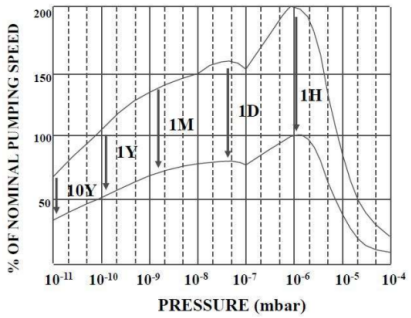


**Figure 3.3:** *The time needed to a SIP to saturate for the different pressures: it increases starting to lower pressures [41]*

with the incoming ion, but after cascade collisions in the target: direct collision would not be able to give to the target atoms an impulse in a direction which would allow them to be ejected. Actually, incident ion collides with the cathode atoms which in turn collide with their neighbors. After every collision the direction of the atoms velocity can change, until one of them acquires a direction pointing out of the target. That is why the incident ions that impact obliquely on the cathode have a larger yield. Moreover, yield increases when projectile and target have a similar mass because the energy is transferred in a more efficient way.

In most cases the sputtered atoms have a neutral charge: since they are not affected by the influence of the electromagnetic field, they can travel freely through the Penning cell (see Fig.3.4).

In low-pressure environment like the one of the ion pump, the sputtered atom has a low probability to scatter with the background gas during its path towards the anode and will settle on the anode forming a film on it. In this way, after some time of pump operation, an active film on anode will form. If the background gas is a reactive gas like $N_2$ or $O_2$, it can form a nitride or oxide layer with this film. This chemical reaction is the main

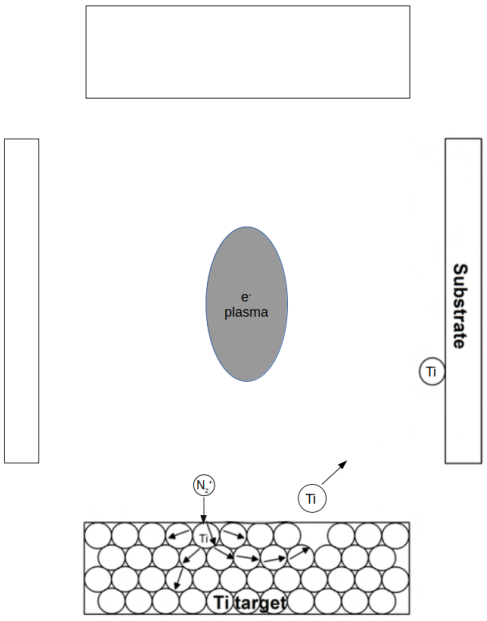


**Figure 3.4:** *The sputter and deposition of sputtered atom process. In this figure an ion of $N_2^+$ collide with the Titanium target. Within it cascade collisions allow to a Titanium atom to be sputtered with a certain velocity until it settles on the anodic substrate*

agent for the pumping process inside a SIP, but the formation of nitrides or oxide layers generate a *poisoned target*, because these layers have a low absorption cross-section with the background gas. This leads to a reduction of pumping capacity by the pump: to recover the lost pumping capacity the Titanium layer must be regenerated with fresh active atoms. Therefore it is fundamental to calculate the sputtering yield in order to understand how quickly the Titanium layer is re-formed. In case of monoatomic metals, semiempirical formulas can be used to calculate the sputtering yield that depends from the energy of the incident ion. In this work the formula devised by Matsunami et al.[30] was used:

$$Y(E) \simeq 0.42 \frac{\alpha^* Q K s_n(\epsilon)}{U_s[1 + 0.35 U_s s_e(\epsilon)]} [1 - (\frac{E_{th}}{E})^{\frac{1}{2}}]^{2.8} \tag{3.13}$$

where $Y$ is the sputtering yield; $\alpha^*$, $Q$ and $E_{th}$ are empirical parameters; $U_s$ is the sublimation energy; $s_n(\epsilon)$ and $s_e(\epsilon)$ are Lindhard's elastic and inelastic reduced stopping cross sections. All these parameters depend essentially from the masses of the target atoms and of the ions and from their atomic numbers. The sputtered atoms are emitted from the surface following the Knudsen's cosine law [27]. In this way it may be possible to calculate the rate of the refreshment of the Titanium layer. To simplify the calculation, it was assumed that the ion hits the cathode in correspondence with the axis of the trap in order to exploit the azimuthal symmetry. This is not a biasing approximation because, as already mentioned before, the electromagnetic field accelerates the ions towards the trap axis.

## 3.3 Conductance

Another quantity useful to calculate the measured pumping speed (see Eq.3.4) is the conductance of the connection tube (see Fig.1.3) between the pump and the volume which has to be emptied. Before talking about the conductance, it is necessary to introduce the boundary conditions which depend from the mean free path of the molecules.

### 3.3.1 Mean free path and Knudsen number

The mean free path is the quantity which describes the average distance between two consecutive molecules collisions. It can be calculated as:

$$\lambda = \frac{1}{\sqrt{2}n\sigma} \tag{3.14}$$

where $n$=$P/k_BT$ is the density of the molecules and $\sigma$ is the elastic cross-section. Some cross-sections are reported in Tab.3.1 for common gases [37].

| **Gas** | **$H_2$** | **He** | **$N_2$** | **$O_2$** | **$CO_2$** |
|---|---|---|---|---|---|
| $\sigma$ (nm$^2$) | 0.27 | 0.27 | 0.43 | 0.40 | 0.52 |

**Table 3.1:** *Cross-sections for different molecules of gas*

The relationship between the mean free path and the physical length scale of the system $D$ which contains the molecules is the *Knudsen number*:

$$K_n = \frac{\lambda}{D} \tag{3.15}$$

The different orders of magnitude of this number define three different gas regimes:

- Free molecular flow ($K_n$>0.5): the interactions between molecules and system walls dominate with respect the interactions between molecules;
- viscous flow ($K_n$<0.01): intermolecular collisions dominate;
- transitional flow (0.5<$K_n$<0.01)

Considering a pipe length scale of the order of 10 cm, systems that are at pressures under $10^{-3}$ mbar are already in free molecular flow. Since the ion pumps have a similar size and they work at lower pressures, their regime is free molecular flow. This is important because in this regime the gas conductance of the vacuum system does not depend on pressure, but only on the mean molecular speed and on the vacuum system geometry.

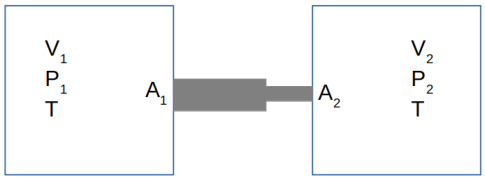


**Figure 3.5:** *An example of a vacuum system composed by two volumes connected by a cylindrical pipe*

### 3.3.2 Conductance calculation in free molecular flow

In a vacuum system with two points at a different pressures $P_1$ and $P_2$ the throughput is equal to:

$$Q = C(P_1 - P_2) \tag{3.16}$$

where *C* is the conductance. If the vacuum system is composed by two different volumes $V_1$ (i.e. the volume to be emptied) and $V_2$ (i.e. the volume of the ion pump) at different pressures $P_1$ and $P_2$, at the same temperature *T* and connected by a cylindrical pipe with a variable section *A*, like the one in Fig.3.5, it is possible to calculate the gas flow from $V_1$ to $V_2$ ($\phi_{1\to2}$) and vice versa ($\phi_{2\to1}$) respectively as:

$$\phi_{1\to2} = \frac{1}{4} A_1 n_1 \bar{v} \tau_{1\to2} \tag{3.17}$$

$$\phi_{2\to1} = \frac{1}{4} A_2 n_2 \bar{v} \tau_{2\to1} \tag{3.18}$$

where *n* is the density of the molecules and $\bar{v}$ is the mean speed of gas molecules. These equations represent the impingement rate of the molecules on the surfaces multiplied by the transmission probability $\tau$ between the

two volumes. If there is no flow, $\phi_{1\to2}$=$\phi_{2\to1}$ and:

$$A_1\tau_{1\to2} = A_2\tau_{2\to1} \tag{3.19}$$

If $\phi_{1\to2}$ is different from $\phi_{2\to1}$, we will have non-zero net flow. Considering the gas law and knowing that $n_1 = N_1/V_1$, $n_2 = N_2/V_2$, with $n_1 \neq n_2$, it is possible to obtain the net flow:

$$\phi_{1\to2} - \phi_{2\to1} = \frac{1}{4}A_1\bar{v}\tau_{1\to2}\frac{(P_1 - P_2)}{k_BT} \tag{3.20}$$

From this equation it is possible to calculate the throughput as:

$$Q = \frac{1}{4}A_1\bar{v}\tau_{1\to2}(P_1 - P_2) = C'A_1\tau_{1\to2}(P_1 - P_2) \tag{3.21}$$

So, comparing this last equation with Eq.3.16 we can obtain the conductance *C* as:

$$C = C'A_1\tau_{1\to2} \tag{3.22}$$

where *C'* is the conductance per unit surface. In Tab.3.2 are reported different C' values for different gases at room temperature [37]:

| **Gas** | **$H_2$** | **He** | **$N_2$** | **Ar** |
|---|---|---|---|---|
| C' at 293K [$ls^{-1}cm^{-2}$] | 43.86 | 31.12 | 11.76 | 9.85 |

**Table 3.2:** *Conductance per unit area for different gases*

For what concern the calculation of the transmission probability, it can be calculated analytically for simple geometries of the pipe such as the cylindrical

shape (which is the most common shape) thanks to the work of Santeler [40]:

$$\tau \simeq \frac{1}{1 + \frac{3L}{8R}(1 + \frac{1}{3(1+\frac{L}{7R})})} \tag{3.23}$$

where $L$ is the length of the cylinder and $R$ is its radius. For more complex geometries the transmission probability can be calculated using the Clausing equations [8] or the test-particle Monte Carlo methods (TPMC), but for the purposes of this thesis it is sufficient to use the Santeler equation.

Now all the elements to calculate the measured pumping speed starting from the ionization pumping speed have been explained. To achieve the goal of this work we now have to calculate the ionization pumping speed, which is proportional to the relationship between ion current and pressure (see Eq.3.3). In the next chapters it will be explained how the ion current will be calculated and simulated.

# Chapter 4

# Simulation study

The ion current calculation in the Penning trap (i.e. in the ion pump) is the heart of the work because, as seen in the previous chapter, ion current is the parameter which allows to understand the performances of the pump (such as the pumping speed). The current is obtained by studying the electron collisions with the background gas in order to extract the relevant parameter, i.e. the frequency of ionizations occurring inside the trap. It is not possible to simply simulate the operation of a full trap, because it contains $10^{10}$ electrons: to simulate all their trajectories would require a too high computing power. The ionization frequency will then be calculated by using the Monte Carlo method starting from the simulation of a single electron generated in a fixed position in a Penning cell. We simulate and follow its trajectory until it collides with the molecules of the background gas or with the electrons of the plasma. Collisions will change the trajectory of the electron and its energy and they will determine its lifetime inside the trap. After simulating one collision we update position and momentum of the electron and we

recalculate its trajectory until the next, up to the total loss of the electron's ability to ionize. Since all these events are random, we can build the electron parameters distributions by running multiple simulations of the life of a single electron. Starting from these distributions we can understand the average behavior of many electrons, which will allow us to calculate the current and pumping speed of the ion pump. The first challenge is to find a way to simulate the electron trajectory inside the trap. This is possible thanks to the work of *Van Gorp et al.* [12], using their tool called Simbuca (Simulation of Ion Motion in a Penning trap with realistic BUffer gas collisions and Coulomb interaction using A Graphics Card).

## 4.1 Simbuca

Simbuca is a modular tool written in $C^{++}$ which allows to simulate the trajectories of a limited number of charges in a Penning trap. This can be done with and without the presence of a background gas. In particular, the user defines the number of particles, their initial conditions (i.e. type of particle, position, velocity, etc.) and the total simulation time; Simbuca divides this time into many sub-intervals, for each of which it calculates step by step coordinates and velocities of the particles in the trap. The modularity of Simbuca is extremely useful because allows the users to modify some of the modules to adapt them to different conditions (as it will be done in this case). The operations performed by the Simbuca tool are reported in [12] and [46]. In this chapter only the Simbuca features relevant to this work will be presented.

```
#
# Input file for Simbuca
# comments can be put in the beginning of the file
#
# Try to simulate electrons in a Penning trap (no buffer gas, no interaction)
#
# Explanation about the input file parameters can be found here:
# http://sourceforge.net/p/simbuca/wiki/Home/#sim-file-parameters
#

CREATEPARTICLES 1
PARTICLES e- 0.0005 0.0005 0.024 0 0 0
TEMP 300
BUFFER 1 1e-4
ODE 4 1 1e-9
COULOMB 0 0
OUTPUT electron_1e-4_real_2 1e-8 0
IDEALTRAP 0.01031 1.4e7 0.13
NE 0.001
```

**Figure 4.1:** *An example of a .sim file. The commands that govern the operation of the simulations are divided in nine lines and allow the users to modify the fundamental aspects of the simulation*

The functioning of Simbuca depends on a series of parameters that are set inside a *.sim* file, such as the initial conditions of the particles, the algorithms to use to calculate the trajectories and the simulation time. When Simbuca is launched by the user, its first operation is to read the *.sim* file. An example of .sim file is shown in Fig.4.1

The lines that start with # are comments, so they have no function on the simulation. The editable parameters are:

- the number of particles to be created at the beginning of the simulation, through the command CREATEPARTICLES. It is followed by an integer which allows to set the number of single particles to create inside the trap;
- the initial parameters of the particles using the command PARTICLES: it is followed by the species of the charges which have to be simulated (in our work electrons *e-*) and from 6 float: the first 3 float numbers indicate the coordinates x, y, z expressed in meters where the charges have to been created. The origin of the reference system corresponds to the center of the Penning cell. The last 3 float numbers indicate the three component of the initial speed of the particles;

- the temperature of the background gas, by using TEMP followed by a float number which is the value of the temperature expressed in Kelvin. This energy is the average value of a Maxwell-Boltzmann distribution;
- the background gas parameters by using BUFFER followed by an integer and a float. The integer can be only 0 or 1 and allows to the user to set or not the presence of a background gas at a certain pressure, expressed in *mbar*, which is set by the float number.
- the numerical method by using ODE followed by 2 integers and a float. The first integer has to be chosen from 0, 1, 4 and 5 and it sets the integrator which calculates the trajectory of the charges considering the forces acting on them. The numerical method to choose from are: Velocity Verlet integrator (0) [52], first order Gear method (1) [53], Runge-Kutta fourth order method (4) [39], Dormand-Prince fifth order method (5) [10, 44]. All these methods differ from each other in the use of adaptive or fixed-value time steps and in simulation time. The adaptive time steps allows to control the uncertainty of the method. This is especially useful in this work because we have to take into account collisions: when an electron is far from the background gas molecule, larger step sizes can be used in order to save time, but when it is about to collide, smaller time steps are needed in order to calculate the position and the speed of the electron immediately before and immediately after the collision. This trajectory sampling allows to study the variation of physical quantities as energies, velocities, positions, etc. with a better accuracy. The numerical method chosen in this work is the Runge-Kutta method because it uses the adaptive

step size and it is quite fast. The second integer allows the user to set (1) or not (0) the adaptive step size and the float number set the time step in seconds. This value is used by the program only if the adaptive step size is disabled;

- the parameters of the Coulomb interaction by using COULOMB followed by two integers: the first one (0 or 1) allows the user to decide if the Coulomb interaction between the charges has to be involved or not. No further details on this factor will be given, as for our purposes the Coulomb interactions are negligible;
- the output parameters, by using OUTPUT followed by a string, a float number and an integer. The output is composed by the main electron information along its trajectory as the position coordinates, the components of velocity, its energy and the time elapsed from its generation. The string is the prefix of the output filename, the float number is the print step, i.e. the time in simulation after which the output is written on file;
- the configuration of the trap, which can be chosen among different options. The two of our interest are:

    1. IDEALTRAP followed by 3 float numbers. In this case, a Penning trap with an ideal electromagnetic field (see Eq.2.1 and Eq.2.2) generated by hyperbolic electrodes (see Fig.4.2) is simulated. The first number sets the radius of the Penning cell in meters, the second one is the constant value $U_0/d^2$ in Eq.2.1 expressed in $V/m^2$ which defines the axial frequency (Eq.2.5) and the third one is the magnetic field value expressed in Tesla;

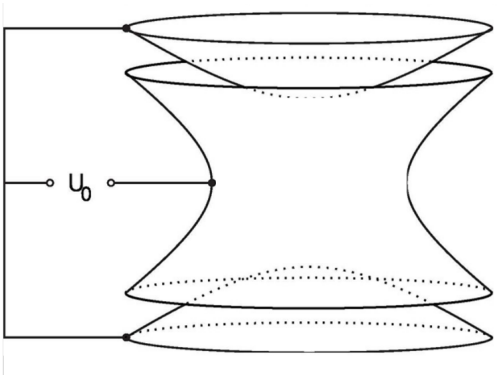


**Figure 4.2:** *An ideal Penning trap with hyperbolic electrodes*

2. REALTRAP allows to the user to use a custom electromagnetic field calculated with other tools (for example COMSOL or OpenFOAM).

- the NE command, which indicates if there are radio-frequencies excitation parameters in the trap. It is followed by a float number which sets the total time to simulate expressed in seconds.

For more details on the other commands it is possible to refer to [46].

An example of an output file produced by Simbuca is shown in Fig.4.3. Our choice was to write a single file containing all the information of the trajectory. At each print step a line is written to the file. Each line contains different data:

- the first one is an integer which represents the number of the particle being simulated. The count starts from the number 0;
- the second is the string with the name of the particle. In this example are considered electrons (e-);
- the next three data are the Cartesian coordinates (x, y, z) of the particle expressed in mm;

```
#Simulation started: Fri May 20 12:42:59 2022
#-------------------------------------------------------------------------------#
#                 Penning Trap Simulation Program by Simon Van Gorp             #
#      Dormand-Prince Runga-Kutta with Proportional Integrating controller      #
#-------------------------------------------------------------------------------#
#index mass x y z (mm) vx vy vz (m/s)    R(mm)           EnergyK(eV)     EnergyP(eV)     EnergyTot(eV)           Temperature(K)          t(ms)
#*******************************************************************************
0 e- 5.000003e-01 5.000003e-01 2.399934e+01 1.019622e+02 1.161042e+02 -2.151677e+05 7.071073e-01 1.316142e-01 2.864287e+03 2.864419e+03 1.527317e+03 6.137797e-09
0 e- 2.862544e-01 6.467179e-01 2.362085e+01 -2.554599e+03 1.069992e+03 -5.154865e+06 7.072380e-01 7.554105e+01 2.791459e+03 2.867000e+03 8.766165e+05 1.000126e-05
0 e- 3.384095e-02 7.064244e-01 2.250714e+01 -2.601667e+03 2.010230e+03 -1.022192e+07 7.072345e-01 2.970389e+02 2.576110e+03 2.873148e+03 3.446989e+06 2.000027e-05
0 e- -2.238246e-01 6.712194e-01 2.064671e+01 -9.204043e+03 -2.238128e+03 -1.528574e+07 7.075542e-01 6.642343e+02 2.219121e+03 2.883355e+03 7.708110e+06 3.000026e-05
0 e- -4.521084e-01 5.447851e-01 1.805069e+01 -1.819708e+04 -5.914619e+03 -2.023331e+07 7.079497e-01 1.163811e+03 1.734112e+03 2.897923e+03 1.350545e+07 4.000047e-05
0 e- -6.212856e-01 3.420787e-01 1.476242e+01 -2.910073e+04 -3.516612e+04 -2.479834e+07 7.092346e-01 1.748216e+03 1.165527e+03 2.913742e+03 2.028718e+07 5.000038e-05
0 e- -7.051897e-01 8.705765e-02 1.084849e+01 -1.602070e+04 -7.092224e+04 -2.844014e+07 7.105431e-01 2.299400e+03 6.193093e+02 2.918710e+03 2.668340e+07 6.000098e-05
```

**Figure 4.3:** *An example of data file produced by Simbuca*

- the next three are the Cartesian components of the velocity expressed in m/s;
- the ninth contains the radial position of the particle expressed in mm;
- the next three data are respectively the kinetic, potential and total energy of the particle expressed in eV;
- the penultimate is the temperature of the particle expressed in K. This value is calculated starting from the electron kinetic energy;
- the last data is the time elapsed expressed in ms.

Data simulated with Simbuca can be graphed by having the output file read by an external tool, which in our case is the Root framework [4].

## 4.2 First tests without background gas

Different tests and modifications of the code have to be implemented before using Simbuca for our goal. First of all, the code is developed to trap positive charges and to eject the negative ones. Since the ion pumps trap electrons, the first step was to modify the force (and so the particle acceleration) calculation in a way to trap the negative charges. After that, we checked if the simulated trajectories are in agreement with theory. To this end, a single electron in an ideal Penning trap was generated at the center of one of the two cathodes. The trap has a radius $\rho_0$ of 10 mm and a distance between

```
#
# Input file for Simbuca
# comments can be put in the beginning of the file
#
# Try to simulate electrons in a Penning trap (no buffer gas, no interaction)
#
# Explanation about the input file parameters can be found here:
# http://sourceforge.net/p/simbuca/wiki/Home/#sim-file-parameters
#

CREATEPARTICLES 1
PARTICLES e- 0.007 0.007 0.013 0 0 0
TEMP 300
BUFFER 0 1e-4
ODE 4 1 1e-9
COULOMB 0 0
OUTPUT electron 1e-8 0
IDEALTRAP 0.010 1.4e7 0.13
NE 0.001
```

**Figure 4.4:** *The .sim file which resumed the initial conditions to simulate a single electron in a way to verify if its trajectory is in agremment with theory*

the cathodes of 49 mm with a negative voltage $U_0$ at the cathodes of 3000 V and an axial magnetic field of 0.13 T. For this test we simulated a completely empty trap (i.e. without background gas). All these conditions are resumed in the *.sim* file in Fig.4.4:

The radial and axial trajectories obtained are shown in Fig.4.5 and in Fig.4.6

To verify if the radial trajectory is qualitatively well reproduced a second simulation decreasing the magnetic field has been done, in order to see if the cyclotron radius increase as expected from Eq.2.13 (see Fig.4.7).

To verify the accuracy of the simulation, a fit of the oscillation frequency is done. As shown in Fig.4.8, the simulated magnetron frequency is about $57.8MHz$ and the theoretical one is about $59.4MHz$. This corresponds to a relative error in simulation of less than $3\%$. For what concerns the oscillation along the axis, the simulated frequency is about $1624.4MHz$ (see Fig.4.9) and the theoretical one is about $1648.9MHz$; so the relative error is less than $2\%$.

The calculation of cyclotron frequency is less straightforward. In Fig.4.5 the cyclotron radius is not visible, because the cyclotron radius is too small to be

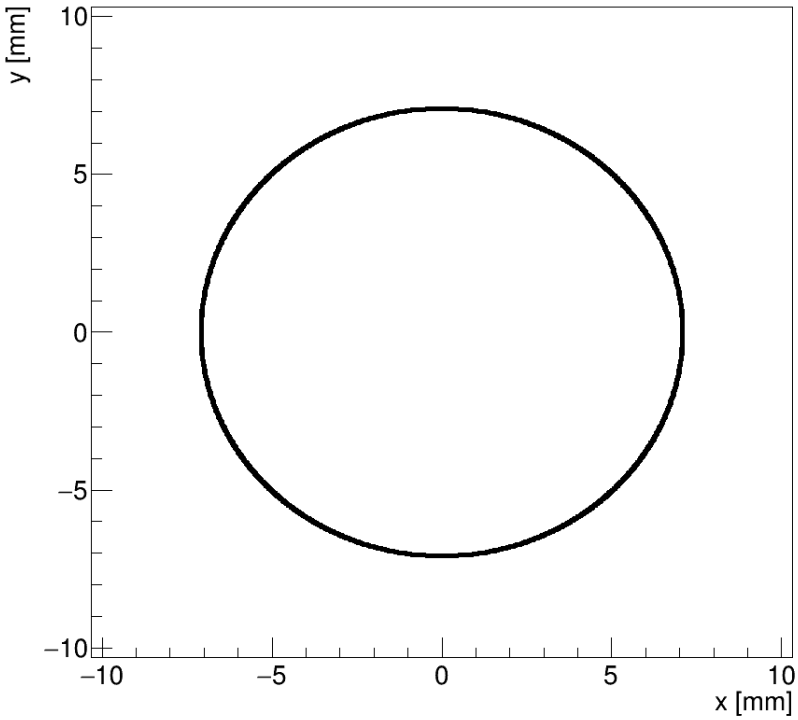


**Figure 4.5:** *The trajectory of a single electron in an empty trap on the radial plane*

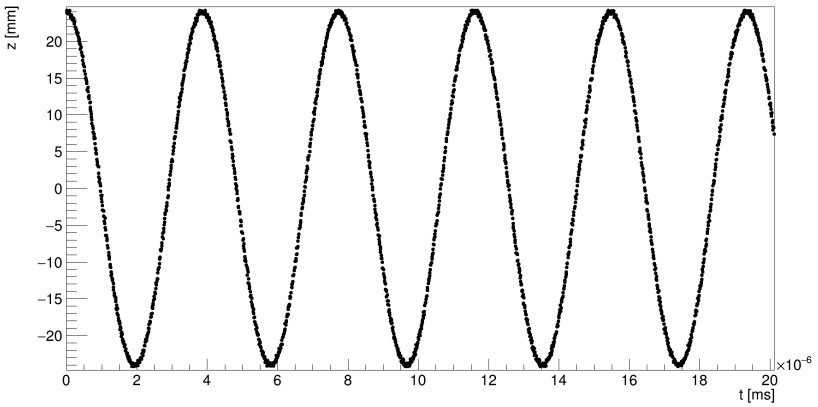


**Figure 4.6:** *The axial oscillation of a single electron in an empty trap*

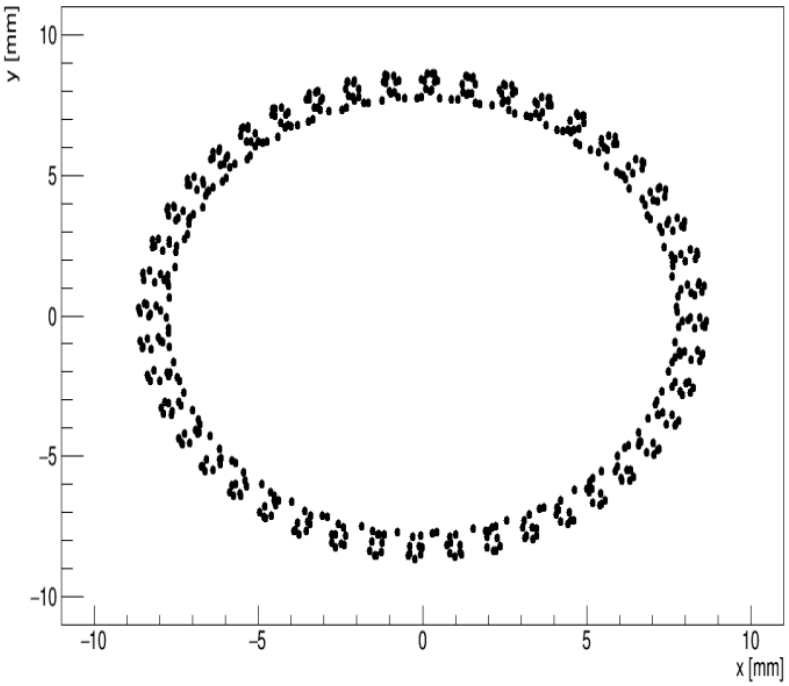


**Figure 4.7:** *The radial trajectory of a single electron with a decreased magnetic field. In this way it is easy to distinguish the slow magnetron oscillation and the faster cyclotron one*

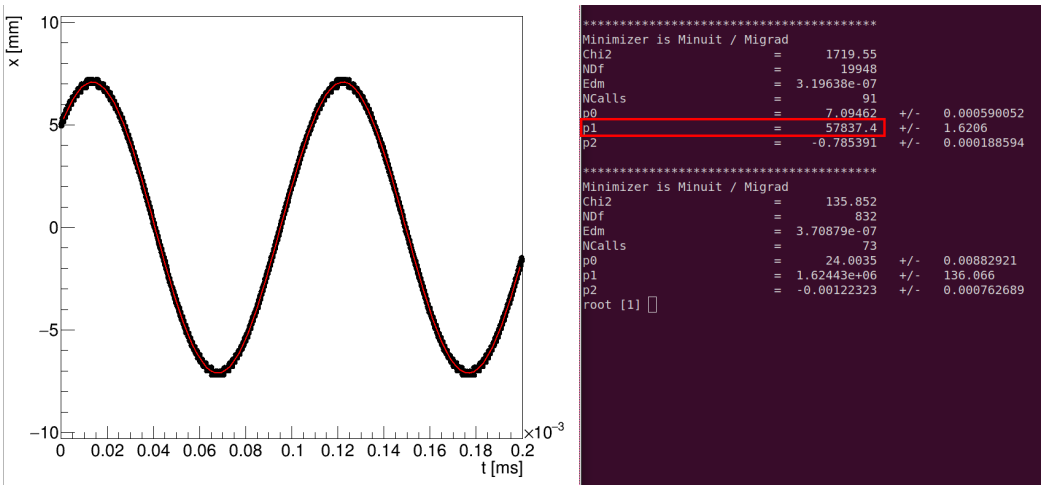


**Figure 4.8:** *The magnetron oscillation of a single electron generated in a trap supplied by 3000 V and with a magnetic field of 0.13 T (left). This frequency is fitted with a sinusoidal function and the frequency obtained is in the red rectangle (right)*

observed using this time scale. So, considering the trajectory for a shorter time with respect to the one reported in Fig.4.8 it is easier to observe the presence of the cyclotron movement (see Fig.4.10)

However, it is still difficult to obtain a good resolution to make a fit.
The only way is to make a new simulation, changing the supply voltage and magnetic field in order to increase the cyclotron radius and decrease the cyclotron frequency. This is done only to understand if the cyclotron trajectory is well simulated. So considering a magnetic field 1000 times lower with respect to the previous simulation the cyclotron trajectory reported in Fig.4.11 is obtained.

In this case the simulated cyclotron frequency is about $22.89 MHz$ and the theoretical one is about $22.86 MHz$. This corresponds to a relative error in simulation of less than $1\%$.

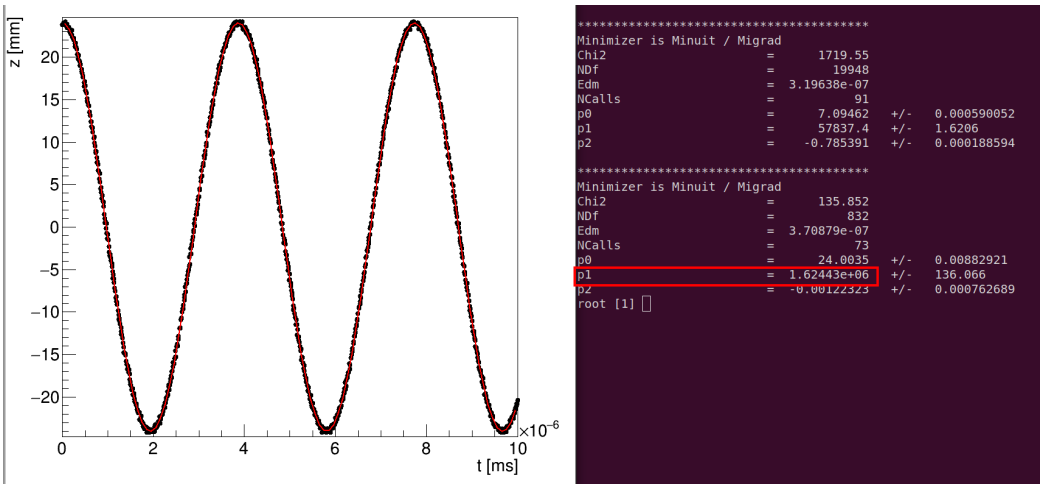


**Figure 4.9:** *The oscillation along the axis of a single electron generated in a trap supplied by 3000 V and with a magnetic field of 0.13 T (left). This frequency is fitted with a sinusoidal function and the frequency obtained is in the red rectangle (right)*

## 4.3 Background gas and implementation of collisions

Simbuca allows to the user to consider the elastic collisions between particles, but unfortunately it does not take into account the ionizations and inelastic collisions. Moreover, it does not calculate the particles deviation after collisions by using the cross-sections. That is why we had to implement an algorithm that does these calculations.

Ideally, a completely empty Penning trap could confine a certain number of electrons forever. Obviously this is not really true, because the trap is never completely empty: there is always a certain quantity of background gas inside it. As mentioned in previous chapters, the presence of a neutral background gas implies the probability of collisions between the trapped charges and the gas itself, which modifies the electrons trajectories and

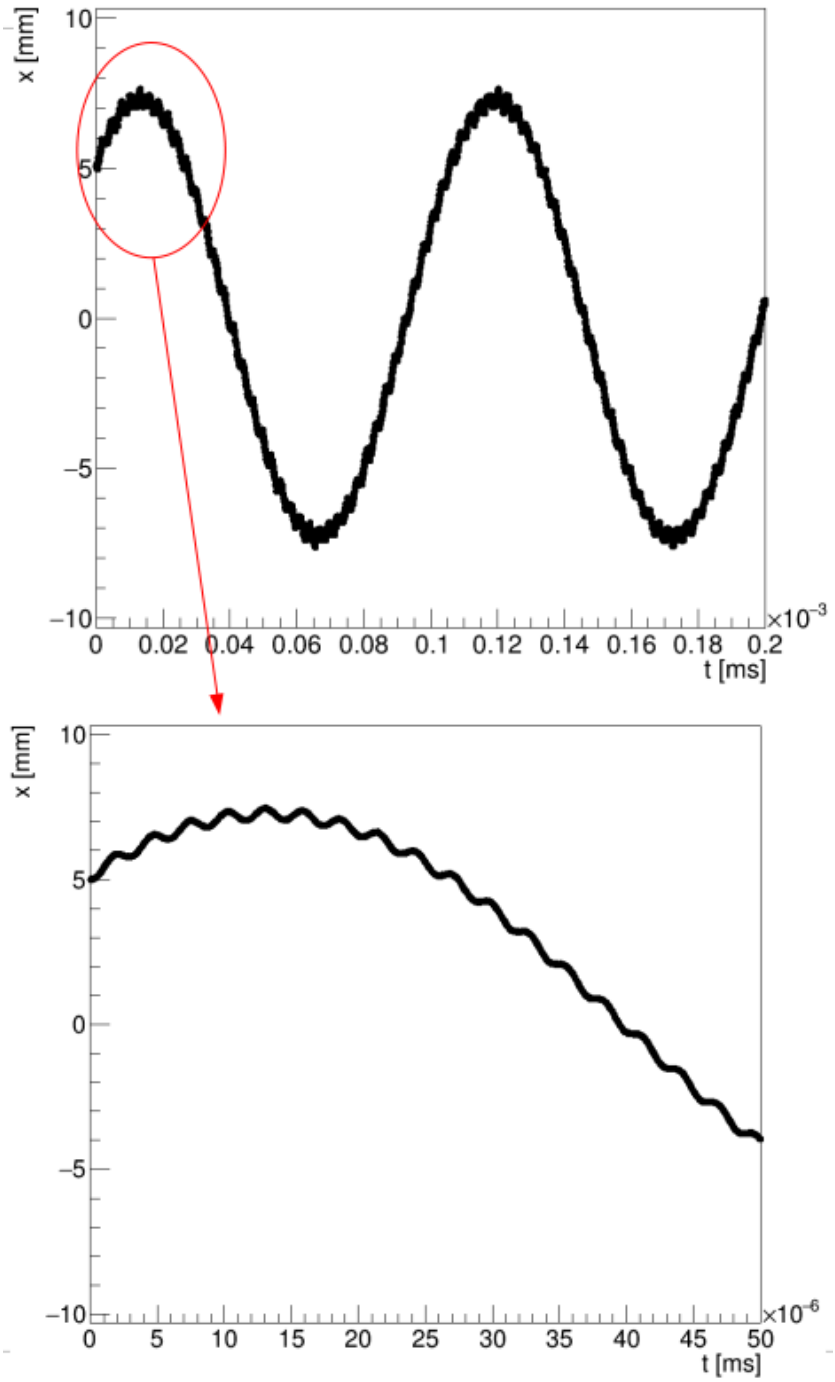


**Figure 4.10:** *A zoom of the magnetron trajectory: it can be observed that the slow magnetron oscillation is composed by a really more fast oscillation with a small amplitude which is the cyclotron oscillation*

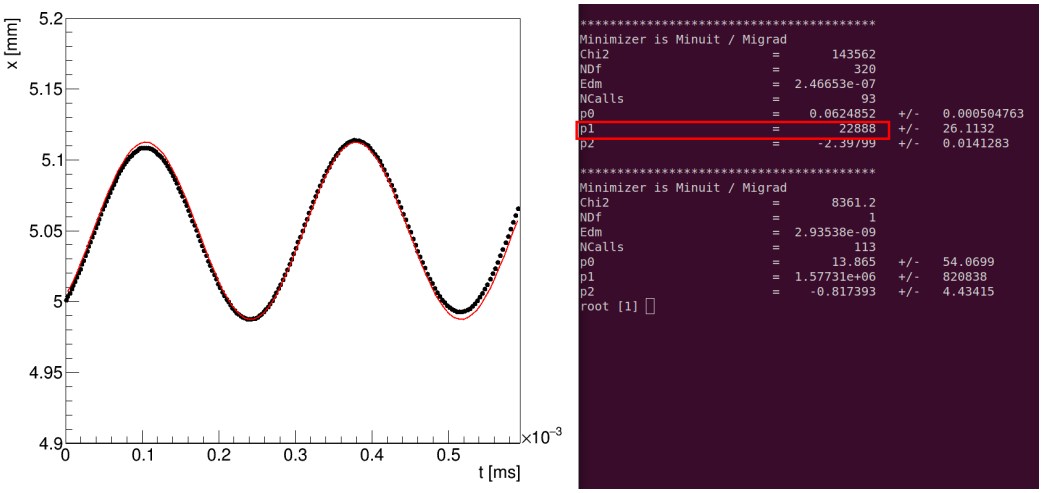


**Figure 4.11:** *The cyclotron oscillation of a single electron generated in a trap with a magnetic field of 0.00013 T (left). This frequency is fitted with a sinusoidal function and the frequency obtained is in the red rectangle (right)*

energies. This leads to a finite confinement time for electrons caused by the loss of energy due to collisions which tend to increase the magnetron radius and lead the electron absorption by the anode. So, it is fundamental for the success of the simulation to be able to correctly consider and simulate the probability of collisions with the neutral gas. This is done considering *the hard-sphere collision model* [2]. This model, in principle, allows to simulate the elastic collisions; however by changing the cross section it can be used to evaluate the probability for inelastic collisions and ionizations.

The collision probability depends from the mean free path $\lambda$.

$$P = 1 - exp(-\frac{v_{\mathrm{e}} \cdot \Delta t}{\lambda}) =$$

$$= 1 - exp(-\frac{\sigma \cdot p \cdot v_{\mathrm{rel}} \cdot \Delta t}{k_{\mathrm{b}} \cdot T}) \tag{4.1}$$

where $v_e$ is the speed of the electron, $v_{rel}$ is the relative speed between

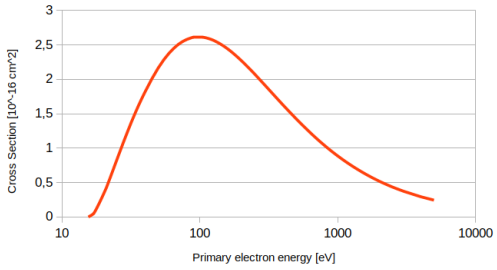


**Figure 4.12:** *An example of cross-sections distribution. In this case is represented the e-$N_2$ ionization cross-section for the different primary electron energies*

the electron and the neutral molecule, $p$ is the buffer gas pressure, $T$ the temperature and $\sigma$ is the collision cross-section. This probability is compared in a certain timestep with a random number (RN) generated between 0 and 1. If P>RN a collision occurs: a random uniform number between 0 and 1 is extracted to decide what type of collision has occurred (elastic, inelastic or an ionization), weighting the outcome with the energy of the electron and the different total cross-sections. The electron velocity after collision is calculated using total energy conservation of the colliding system and the new direction is chosen using the differential cross section (as it will be explained shortly). Therefore, knowing which gas is present inside the trap, it is possible to calculate the probability that a certain electron-gas collision will occur by using the cross-sections distributions (see Fig.4.12). In this work only two gases are considered as background: $H_2$ and $N_2$. The cross-sections used in these simulations are studied in [16, 21, 22, 24, 29, 31, 33, 45].

Moreover it is fundamental to locate the collisions temporally. As mentioned before Simbuca produces data output (which contains information about position, velocity, energy, etc.) after simulating a certain period of time which

```
1 #index x[m] y[m] z[m] vx[m/s] vy[m/s] vz[m/s] Ek[eV] Ep[eV] Utot[eV] time[s] collision theta phi thetap phip
2 0 -0.000283279 0.000648172 -0.0232549 -1438.95 -10644.7 -7.22493e+06 148.394 2719.95 2868.35 3.18199e-08 E 0.244253 1.94428 -10 -10
3 0 -0.000147568 -0.000502649 -0.0236444 3.16837e+06 3.75179e+06 886964 70.7894 2795.92 2866.71 7.6134e-08 E 0.236521 1.53361 -10 -10
4 0 0.000858302 -0.000104855 -0.0158323 4.43008e+06 2.26955e+06 2.29461e+07 1567.25 1343.65 2910.9 1.35621e-07 I 1.37649 0.999165 1.3061 2.95868
5 0 -0.00158948 0.00120062 -0.0143162 -1.73328e+07 1.0492e+06 -9.62772e+06 1120.69 1086.28 2206.97 1.94622e-07 E 0.102343 3.82302 -10 -10
6 0 -0.00198871 -0.000511067 -0.0180022 3.4347e+06 5.64228e+06 -1.09804e+07 466.792 1720.83 2187.62 2.17011e-07 I 1.73516 2.17759 2.00366 2.62202
7 0 -0.000209037 -0.00129301 -0.0148939 -5.3666e+06 6.8948e+06 1.39984e+07 774.084 1183.6 1957.69 2.40435e-07 E 0.0587364 0.97273 -10 -10
8 0 0.00103855 0.000872175 0.0162849 1.28171e+07 -3.75731e+06 -3.08925e+06 534.273 1417.09 1951.36 2.97276e-07 E 0.086716 0.445045 -10 -10
9 0 -0.000433082 0.00213055 -0.0108796 -6.05585e+06 -9.72419e+06 -1.86195e+07 1358.63 600.776 1959.41 3.12408e-07 E 0.0456377 3.97721 -10 -10
10 0 -0.00318588 0.000294209 0.0111643 1.99669e+07 -8.15825e+06 3.05916e+06 1349.18 610.42 1959.6 3.33896e-07 I 1.68406 3.76614 2.39417 5.76486
11 0 -0.00237259 -0.00128646 0.0113209 -7.26431e+06 1.08305e+07 184324 483.572 643.122 1126.69 3.48622e-07 I 1.69286 0.371774 1.5969 0.491302
12 0 0.000502977 -0.00291151 -0.00429269 -2.45469e+06 6.92247e+06 -1.41661e+07 723.847 152.704 876.552 3.68898e-07 E 0.0165483 1.9583 -10 -10
```

**Figure 4.13:** *An example of collisions file*

is set in the .sim file. However, this period of time is too long to account precisely for the collisions, because most of them are likely to occur before this time. So, Simbuca was modified in order to produce a second file, in which is highlighted what kind of collision occurred and where it is located physically and temporally. The file which contains the collisions information is shown in Fig.4.13.

This file contains the following information:

- the first column is an integer relative to the number of the particle that underwent the collision;
- the next three numbers are the Cartesian coordinates where the collision is occurred expressed in m;
- the next three numbers are the Cartesian components of the velocity expressed in m/s an instant before the collision;
- the next three numbers are respectively the kinetic, potential and total energy expressed in eV before the collision;
- next, there is the exact time when the collision occurs (expressed in s) independently from the value of the output file set in the .sim file;
- next, there is a string that contains what type of collision is occurred: *A* is for inelastic collisions, *E* is for elastic collisions, *I* is for ionizations, *ee* is for electron-electron collisions (see 4.6), *T* is for electron-upper cathode collisions, *B* is for electron-lower cathode collisions, *W* is for

electron-anode collisions;

- the last four columns are angles expressed in rad. The first two are respectively the $\theta$ and $\phi$ angle to which the primary electron will be deflected with respect its direction. Instead the last two columns are the $\theta$ and $\phi$ angle with respect the primary electron direction to which the secondary electrons generated in case of ionization will be directed. If the collision considered is not an ionization, these last two angles are set at the value -10.

This file is read and analyzed by the Root framework in order to integrate the information on trajectories with information on collisions.

### 4.3.1 Conservation and loss of energy

Our primary purpose is the calculation of the current inside the Penning trap. This value is proportional to the number of ionizations happening inside the pump. Therefore, it is essential to understand how the energy of the electron varies in order to understand how many ionizations it can do. So, we have to calculate the loss of energy after collisions. Moreover, this study allows us to verify the accuracy of simulation by checking the conservation of the total energy and the distribution of the kinetic and potential energy in the trap. Total energy is constant when the electron is not disturbed by collisions, but after an inelastic scattering or ionization it loses a part of its total energy. To calculate this energy loss a random value from a Landau distribution (that governs the loss of energy) is extracted and is subtracted from the kinetic energy of the electron [28]. The Landau distribution is centered around half

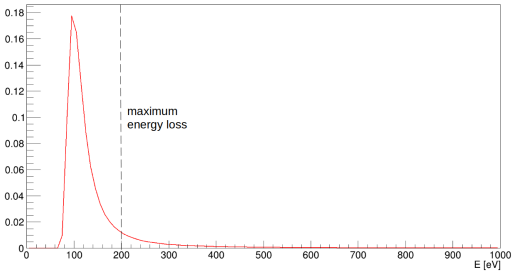


**Figure 4.14:** *Example of a Landau distribution centered at the half of the electron kinetic energy that is about 200 eV. In this case this value corresponds to the maximum possible energy loss.*

of the electron kinetic energy and has a sigma of 10% of this energy. The maximum possible energy loss is equal to the kinetic energy of the electron. If the energy loss extracted from the distribution is bigger than the kinetic energy, the loss value is considered equal to the kinetic energy. An example of Landau distribution is shown in Fig.4.14.

The energy distributions of the electrons, taking into account the collisions and the energy loss due to them, are obtained by simulating a single electron 500 times. The electron is always generated near the cathode in a trap with a supply voltage of 3 kV and with a magnetic field of 0.12 $T$. Since the electron is generated close to the cathode, its potential energy (and the total one) is determined by the voltage at the cathode. The electron is generated at the cathode at rest: this approximation does not affect the simulation results, because these electrons represent the ones emitted from the cathode after ion-cathode collision. Even if in reality these electrons have a small kinetic energy, it is much lower than the potential energy, therefore, for simplicity, their initial speed is approximated to zero. The background gas considered is $N_2$ at the pressure of $10^{-6}$ mbar. As mentioned before, Simbuca produces the position and speed of the electron with a certain time step. Starting from the

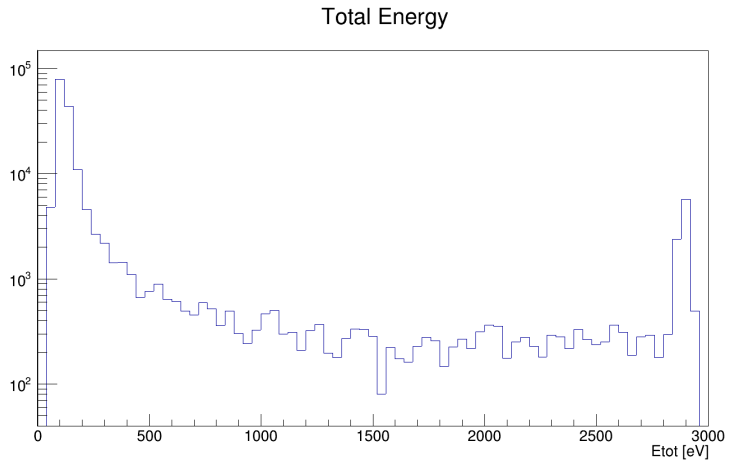


**Figure 4.15:** *The total energy distribution sampled in all time steps of the 500 simulations*

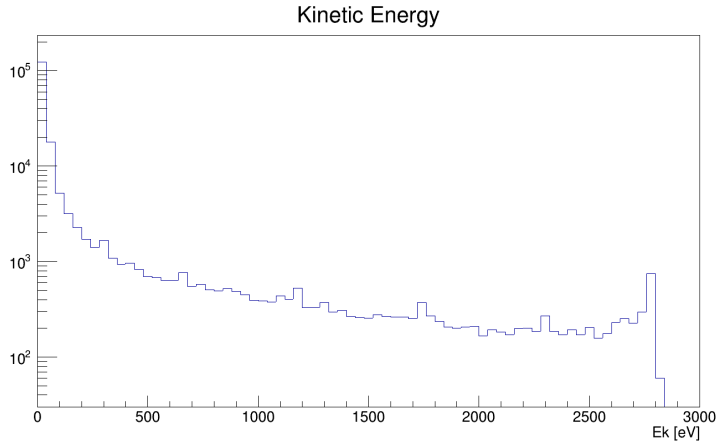


**Figure 4.16:** *The kinetic energy distribution sampled in all time steps of the 500 simulations*

speed and position we can determine its total energy. These energies are not constant because of collisions. Therefore, considering the entire trajectory, the total and the kinetic energy distributions in the various time steps in all 500 simulations are reported from Fig.4.15 to Fig.4.20. Instead in Fig.4.21 and Fig.4.22 are reported the total energy distributions in the various time step for a single simulation, i.e. the energy sampling of a single trajectory.

From these distributions it is possible to make the following considerations:

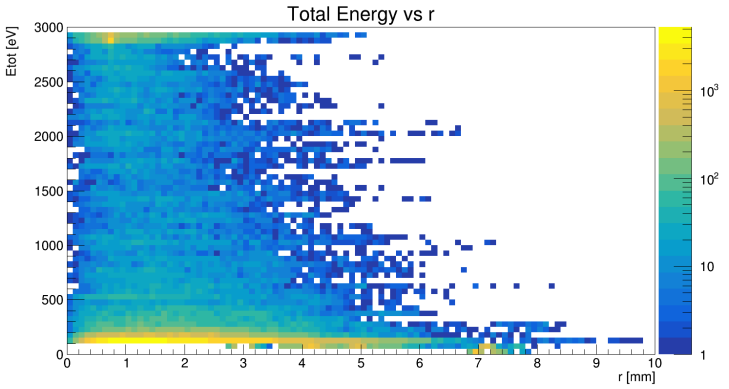


**Figure 4.17:** *The total energy, sampling all the 500 electron trajectories, with respect to the radial position inside the trap*

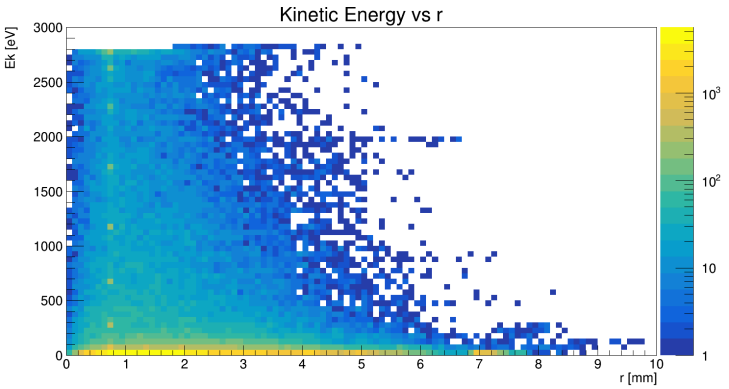


**Figure 4.18:** *The kinetic energy, sampling all the 500 electron trajectories, with respect to the radial position inside the trap*

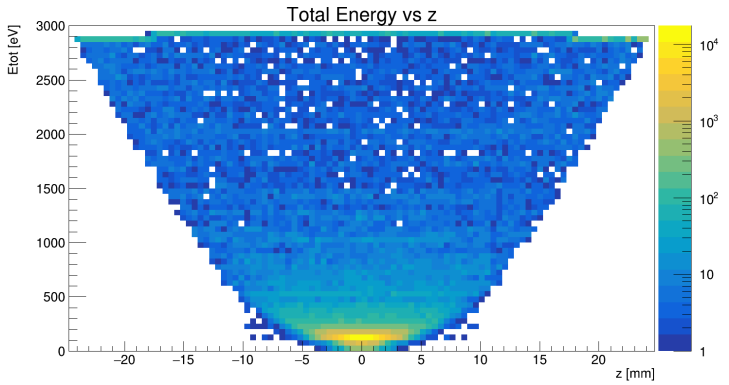


**Figure 4.19:** *The total energy, sampling all the 500 electron trajectories, with respect to the axial position inside the trap*

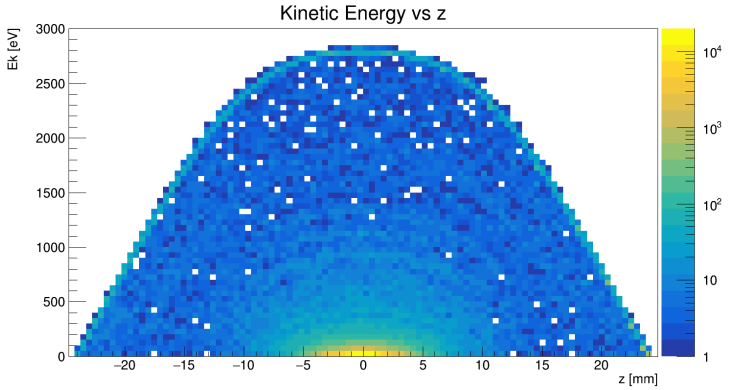


**Figure 4.20:** *The kinetic energy, sampling all the 500 electron trajectories, with respect to the axial position inside the trap*

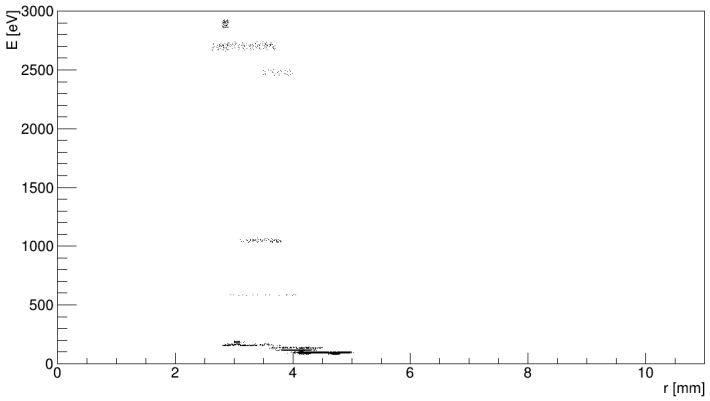


**Figure 4.21:** *The total energy, sampling a single electron trajectory, with respect to its radial position inside the trap*

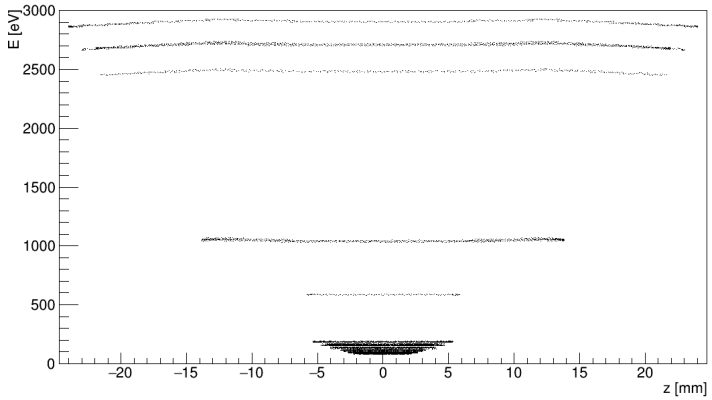


**Figure 4.22:** *The total energy, sampling a single electron trajectory, with respect to the axial position inside the trap*

- the electron spends most of its life inside the trap having a low energy;
- in Fig.4.17 and Fig.4.18 there are white zones, i.e. radial coordinates of the trap not accessible to electrons which have a certain energy. This is because the further electrons are from the axis of the trap (i.e. closer to the anode), the more intense the radial component of the electric field is. Therefore the more energetic electrons, when they enter these zones, are accelerated out of the trap. Near the anode are located only the electrons with a low energy, i.e. those that have lost a lot of energy via collisions (see 2.1);
- the white zones in Fig.4.19 and Fig.4.20 represent the axial coordinates not accessible from electrons with a certain total and kinetic energy. This because the maximum total energy is linked with the maximum potential energy. Since the maximum axial oscillation depends on the potential energy, then we can say that the oscillation amplitude is proportional to the total energy and vice versa: the lower the total energy of the electron, the lower will be its axial oscillation amplitude. From that distributions it is clear that the electrons spend a lot of their time in the trap with a low energy and with a small axial oscillation amplitude;
- in Fig.4.21 and Fig.4.22 it is possible to observe that the total energy is divided into bands because, as explained before, it stays constant until an ionization or inelastic collision occurs (conservation of energy respected);
- the simulated energy distributions follow the theory prediction (see 2.1).

### 4.3.2 Angle calculation from differential cross-sections

Electron scattering is fundamental because influences the transfer of energy and its trapping time. These two parameters have a central role in ion current calculation because the number of ionizations made by a single electron depends on them.

As seen before, the energy of an electron inside the trap depends on the position it occupies. An electron with a certain total energy, after the collision can be deviated in position where the potential energy is lower or higher with respect to the potential energy at the position where the collision occurred. Moreover the change in direction can lead to a "redistribution" of the kinetic energy: an electron with an axial velocity much greater than the radial velocity can be deflected by the collision in a way to have a predominantly radial speed. In this way the kinetic energy, which before the collision was mainly due to the axial motion, after collision is mainly associated to the radial oscillation. Trapping time is also related to scattering, as the new direction after the collision brings the electron radially towards or away from the anode. In this way the radial intensity of the electric field acting on the electron changes, influencing its time inside the cell: the closer the electron is to the anode, the stronger the electric field will push it toward the wall.

Now we will analyze how to calculate the scattering angle. When a collision between particles occurs, they are deviated by a certain angle with respect to their direction of motion. This angle depends on several factors such as the mass of the particles, their energies etc. It is well known that if one particle has a much greater mass than the other one, its deviation due to the collision

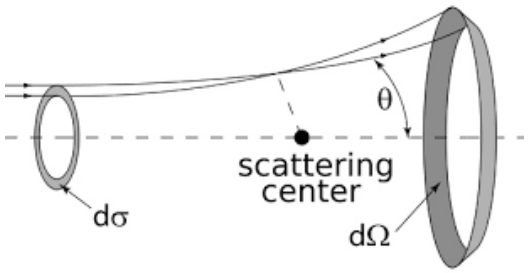


**Figure 4.23:** *The schematic collision between two particles where the target has a much greater mass with respect to the electron which will be deviated of a certain quantity dΩ.*

can be neglected. Since the collisions in an ion pump are between electrons and molecules we will neglect the deviation of molecule (see Fig.4.23).

The deflection after the collision in space depends from the azimuthal $\phi$ angle (between 0 and $2\pi$) and the polar $\theta$ angle (between 0 and $\pi$). After every collision the deflection angles have to be recalculated. When a collision occurs, we put our reference system at the point of impact and we consider polar coordinates. The angles will be calculated with respect to the electron direction. Due to the symmetry of the fields there is no reason to have a privileged direction in $\phi$ direction, therefore its value after the collisions can be uniformly extracted between 0 and $2\pi$. The same is not true for the $\theta$ direction which depends from different factors as the energy of the primary electron, the type of particles etc. As seen previously, a shift along the polar angle leads the electron to occupy a different axial position which corresponds to a different potential energy. The probability to have a certain scattering polar angle, for the different particles, is expressed by the differential cross-section. In particular a primary electron with a certain energy has different probabilities of being deflected by a $\theta$ angle. In Fig.4.24 and Fig.4.25 are shown respectively the differential cross-sections for e-$N_2$

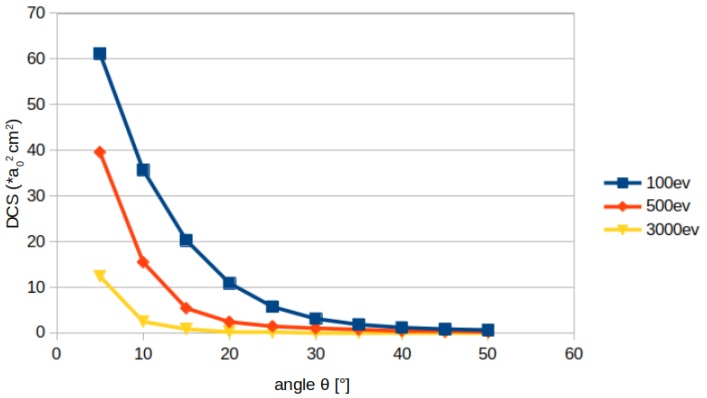


**Figure 4.24:** *The differential cross-sections distributions for elastic e-$N_2$ collisions where the primary electrons have different energies*

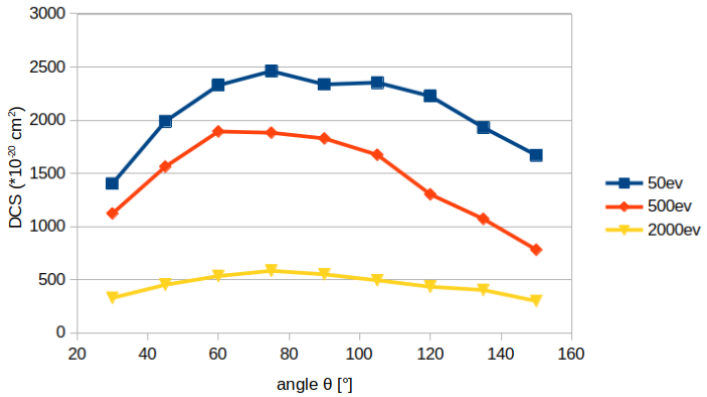


**Figure 4.25:** *The differential cross-sections distributions for e-$N_2$ ionizations where the primary electrons have different energies*

elastic and ionizing collisions for primary electrons with different energies. For higher electron energies, flatter distributions resulted.

Ionizations cross-sections for a primary electron at a certain energy take also into account the different probabilities to emit a secondary electron at a certain energy and angle. All the secondary electrons are considered generated at rest as discussed in [23] and [19]. So the ionizations differential cross-sections distributions are obtained integrating over all possible secondary electron emission angles at a certain energy.

Polar angle distributions at different energies are parameterized using an exponential function for the elastic collisions and a polynomial function of the fifth order for the ionizations.

Cross-sections are given for discrete values of energy, but the primary electron energy can take on any value within the spectrum. Then, to obtain the cross section corresponding to the energy of the electron, an interpolation is made between the two curves referring to the two discrete energy values between which our electron energy lies.

### 4.3.3 Particle trajectories

The last check that must be done to understand if the algorithms implemented by us in Simbuca (i.e. ionization and inelastic scattering and loss of energy) work correctly, is the verification of the electrons trajectories in presence of a background gas. This is done by verifying the variation of the radial and axial coordinates over time. If their variation follows the theoretical principles we talked about in the previous chapters, then the single trajectory of the electron is well simulated. Since it is linked to the transfer of energy, a correct trajectory require accurate simulation of the exchanges of energy in order to evaluate the number of ionizations which take place inside the trap. Considering a set of simulations with the same conditions reported in the previous section ($U_0 = -3kV$, B=0.12 T), the radial and axial coordinates variation over the time are shown in Fig.4.26.

These coordinates distributions are in agreement with what is explained in 2.2, i.e. a tendency of the magnetron radius to increase and a tendency of

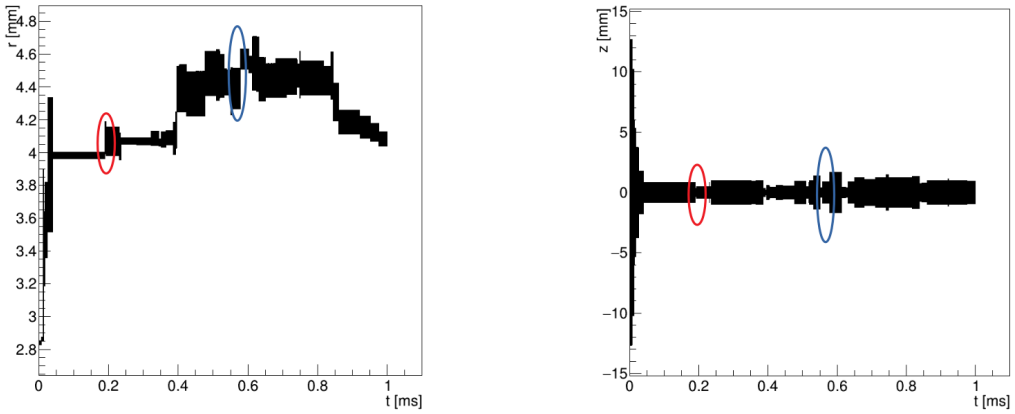


**Figure 4.26:** *The variation of the radial coordinates (left) and the variation of the axial coordinates (right) for a single electron with respect to the time*

the axial oscillation amplitude to decrease with increasing collisions and energy loss. Observing the distribution of the radial coordinates over the time, the thickness of the curve along the vertical direction represents the cyclotron radius at a certain time (of which an enlargement is shown in Fig.4.27), while the average value is the magnetron radius. This should be more clear by referring to the Fig.4.7 and Fig.4.5 where we reported the electron radial trajectory in an empty trap (i.e. without collisions). In that case the trajectory is simulated for a short time in order to allow the electron to complete one revolution around the trap axis. But if we imagine to graph that radial coordinates for a longer time, we would see a constant line at a certain value (corresponding to the magnetron radius) with a certain constant thickness (corresponding to the cyclotron radius). After collisions, the magnetron and cyclotron radiuses change, but the interpretation of the quantities is always the same.

Observing the radial coordinates variation it can be seen that in the first moments of life of the electron, its magnetron radius increases faster than

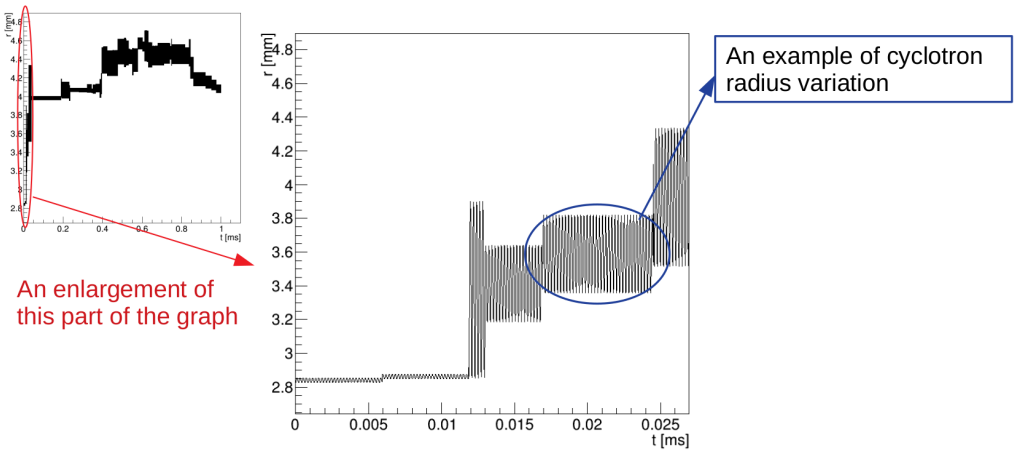


**Figure 4.27:** *The zoom of the variation of the radial coordinates over the time shows that the thickness of the line contains the cyclotron oscillation*

later. This is connected to the energy loss. As we said before, after an inelastic or ionization collision the electron loses an amount of energy that follows a Landau distribution centered around half its kinetic energy. Therefore in its first moments of life the energy lost will be statistically greater, as the electron have more energy and this is reflected in a greater increase in the magnetron radius. In Fig.4.26 it is possible to see that the variation of the cyclotron radius is inversely correlated to the variation of the amplitude of oscillation on the axis (conservation of total energy).

## 4.4 Electric field simulation using OpenFOAM

Until now all the simulations were obtained taking into account simulations with the ideal electromagnetic field expressed by the Eq.2.1 and Eq.2.2. But in order to obtain more precise data it was decided to consider an electric field that was as similar as possible to the real one. Moreover, as mentioned before, Simbuca has the ability to simulate the particles trajectories starting from

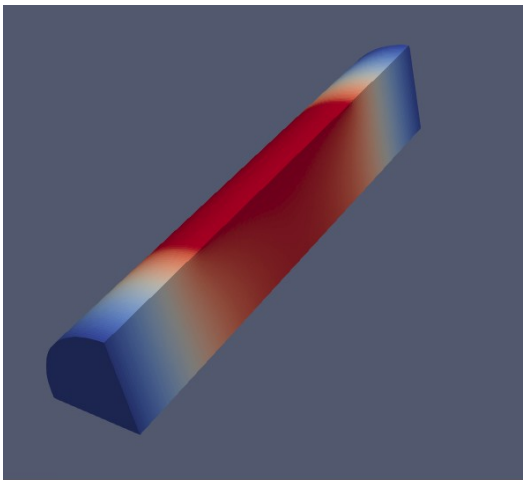

**Figure 4.28:** *The electric potential simulated in the quarter of the Penning cell: the blue in correspondence of the cathodes is equivalent to a potential of -3000 V, while the red in correspondence of the anode is equivalent to the ground state*

external electromagnetic field data, knowing its radial and axial coordinates. It is well known that there are several commercial tools which allow one to simulate the electromagnetic field in a certain volume of space starting from the geometry of the electrodes. OpenFOAM was used in this work for the electromagnetic field simulation [54]. It is a free open source tool mainly used in the computational fluid dynamics (CFD). Solving a problem using this tool consists of several steps: pre-processing, solving, post-processing. Thanks to it, is possible to calculate the electric field and its potential: the result is shown in Fig.4.28

OpenFOAM allows to save these data in a text file which is read by Simbuca before the start of the simulation. After reading this file Simbuca creates a map of the field: it creates a discrete set of coordinates $r$ and $z$ inside the trap (in our case the distance between two discrete points is of the order of $10^{-5}m$ for the radial points and $10^{-4}m$ for the axial ones) and it associates

the corresponding value of the electromagnetic field read from the text file. After do this, the simulation start. When the electron is in an intermediate position with respect to the discrete coordinates, an algorithm performs a linear interpolation for the calculation of the specific field and potential for its location. Further details on OpenFoam are given in the Appendix.

## 4.5 Influence of plasma in the trap

In this section we will describe how we treat the plasma effects in our simulation. We will have to take into account both its influence on the electric field and the probability that the plasma electrons collide with the active ones, whose trajectory we want to simulate.

Our understanding of plasma formation and effects start from the principles expressed in 2.3, for which, after a certain number of collisions, the electrons are confined in the central region of the trap due to the loss of energy which reduces the amplitude of axial oscillation. This leads to a concentration of charges which affects the electric field in a not negligible way. To take this effect into account, we hypotize the presence of a cylindrical-shaped plasma region inside the trap, with almost the same radius of the cell, centered on the center of the trap and extending for 4 mm along the axis (see Fig.4.29). The axial extension of 4 mm is chosen because it corresponds to the axial oscillation of an electron whose total energy is slightly lower than the energy needed to ionize one molecule. This approximation allows to calculate in an easy way the effect of the space charge in a Penning cell and its influence on the parameters needed to calculate the current and pumping speed, such

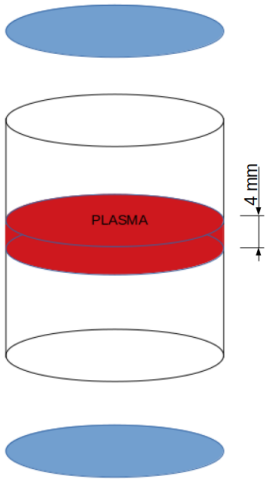


**Figure 4.29:** *Plasma model inside the trap*

as the number of ionizations, the average life of the electron inside the trap and the ionization frequency. In the next chapter we will explain how we will use these parameters to calculate the current.

In reality, according to [11] the plasma shape due to the ionizing discharge of the electrons may be that of a prolate ellipsoid with a radial extension of a few *mm* and axial extension approximately equal to the distance between the cathodes, therefore one would think that our approximation is completely wrong. However, as we will see in 5.2, the shape of the plasma does not considerably change the distributions of the parameters needed to calculate the current, whereas its count is influenced only by the volume of the plasma and not by its shape. Furthermore, in Dubin's studies [11] the ellipsoidal shape of the plasma is calculated for electrons having enough energy to ionize; but in our specific case we must consider that there is also a large number of electrons with a low energy (i.e. unable to ionize) which occupy the central region of the trap that we have considered as cylindrical. Therefore, since we

do not know the exact proportion between the low energy electrons (which occupy the cylindrical volume) and the high energy ones (which should be arranged occupying the ellipsoidal volume) and since, as we will see later, the cylindrical plasma gives good agreement between the values of current simulated and measured, in this first version we will consider the plasma as a cylinder. A more in-depth study of the shape will be done in future studies. So, at this point, the simulation has to consider the probability that an active electron (i.e. with an energy greater than the ionization energy) collides with an electron in the plasma.

## 4.6 Electron-electron collisions

When a highly energetic electron passes through the electron plasma, it loses energy through electron-electron collisions. In order to simulate these interactions, their total and the differential cross-sections are calculated using the Moller scattering formula [49]:

$$\sigma \simeq \frac{0.0342}{(E_{\text{cm}}/GeV)^2} mb \tag{4.2}$$

$$\frac{\partial \sigma}{\partial \Omega} \simeq \frac{\alpha^2}{{E_{\text{cm}}}^2 sin^4\theta} \cdot (3 + cos^2\theta)^2 \tag{4.3}$$

where $\alpha = \frac{q^2}{4\pi}$, $E_{cm}$ is the center-of-mass energy expressed in *GeV* and $\theta$ is the polar angle of the scattered electron. Eq.4.2 is obtained considering identical particles in the final state starting from Eq.4.3 [49] and its result is expressed in *millibarn*. The collision cross-sections allow to calculate the

probability of the collision (see Eq.4.1) and the direction of the primary electron after the collision. In this way, all the elements that can affect the life time of an electron are taken into account.

## 4.7 Parameters distributions

Simulate the pump operation by tracking step by step all the trajectories and interactions of all the electrons with molecules, plasma electrons and trap walls is impossible due to the high number of electrons inside the trap, but it would be also useless. What we need to know is how many ionizations an electron induces, its ionization frequency and its life time (i.e. the time that passes from when the electron is generated until it either hits a wall of the trap or it reaches the energy threshold where it can no longer ionize). These parameters are closely related to the calculation of the ion current because they told us how many ions are generated by a single electron during its life. After obtaining the parameters distributions it will be possible to implement a new simulation which, using those distributions, will allow us to simulate the current and pumping speed without sampling all electrons trajectories step by step.

To obtain the statistic distributions of these parameters we simulates some hundred times (500 o 1000 according to the background gas pressure considered) the entire life of a single electron following their trajectories every time step. These electrons are generated near the cathode as they are the ones that have the greatest possible energy and therefore contribute most to the ionizations that take place in the trap. We know that also the secondary

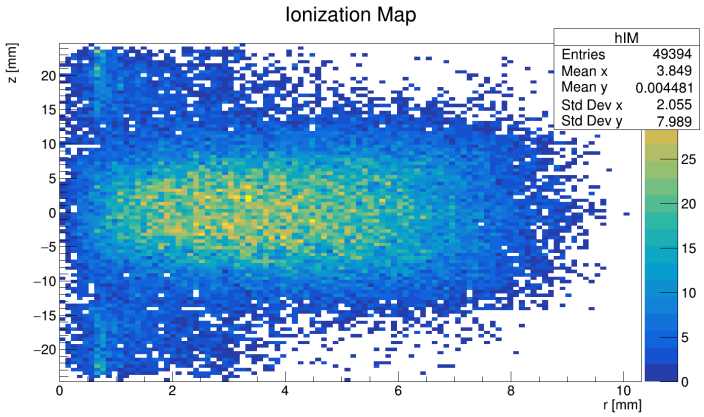


**Figure 4.30:** *Ionization map: the r and z coordinates inside the trap where the ionizations occur. This map is obtained considering all ionizations in 500 simulations of a single electron with $N_2$ as background gas at a pressure of $10^{-6}$ mbar. From this map we can see that the electron-ion pairs are generated in the central area of the trap*

electrons generated during the ionizations may contribute to the electric discharge, but as we can see in Fig.4.30 (which represents the coordinates where ionizations occur) they are created mostly in the central trap area where the potential energy is much less than the one of the electrons which are near the cathode.

Since, as already explained previously, the secondary electrons are generated with zero kinetic energy, their total energy will be much lower than the one of the electrons generated at the cathode, contributing less to the number of ionizations. That is why, in this first version of the simulation we take into account only the electrons generated near the cathode. The inclusion of secondary electrons in the calculation of ionizations will be developed in future versions of the simulation.

Instead, for what concern the ions generated during the ionization, they are accelerated towards the center of one of the two cathodes due to the electromagnetic field. The ion-cathode collision generates an electron [25] with

a potential energy determined by the cathode potential (i.e. the maximum allowed electron energy inside the trap). This is the initial condition of the simulated electrons from which the parameters listed above were extracted. As said before all of these parameters depend on background gas pressure. To determine these distributions with a good statistics for the pressures equal or larger than $10^{-7}$ mbar 500 simulations were launched, while for lower pressures, 1000 simulations were launched. From that simulations the time between two consecutive ionizations, the number of ionizations made from each electron and life time were extracted (see Fig.4.31, Fig.4.32 and Fig.4.33). This is repeated for a discrete set of pressures values. Actually, simulations were performed using a collision probability increased by six orders of magnitude (i.e. a pressure and a plasma density six orders of magnitude greater) in order to reduce the calculation time, and the results were then re-scaled to the relevant pressure and density.

Looking at the distributions we note that the average values of the electrons life time and of the time between two ionizations change linearly with the pressures while for what concerns the multiplicity its average value is more or less stable at different pressures. These behaviors are due to the fact that any change of the pressure of the background gas, modifies accordingly the probability to have a collision (see Eq.4.1) and consequently the life time. On the other hand, ionization multiplicity depends from the energy of the electron; the loss of energy of the electron after a single collision is not affected by the molecules density.

When all parameters distributions are obtained, another set of simulations is launched. The aim of these ones is to understand how the number of

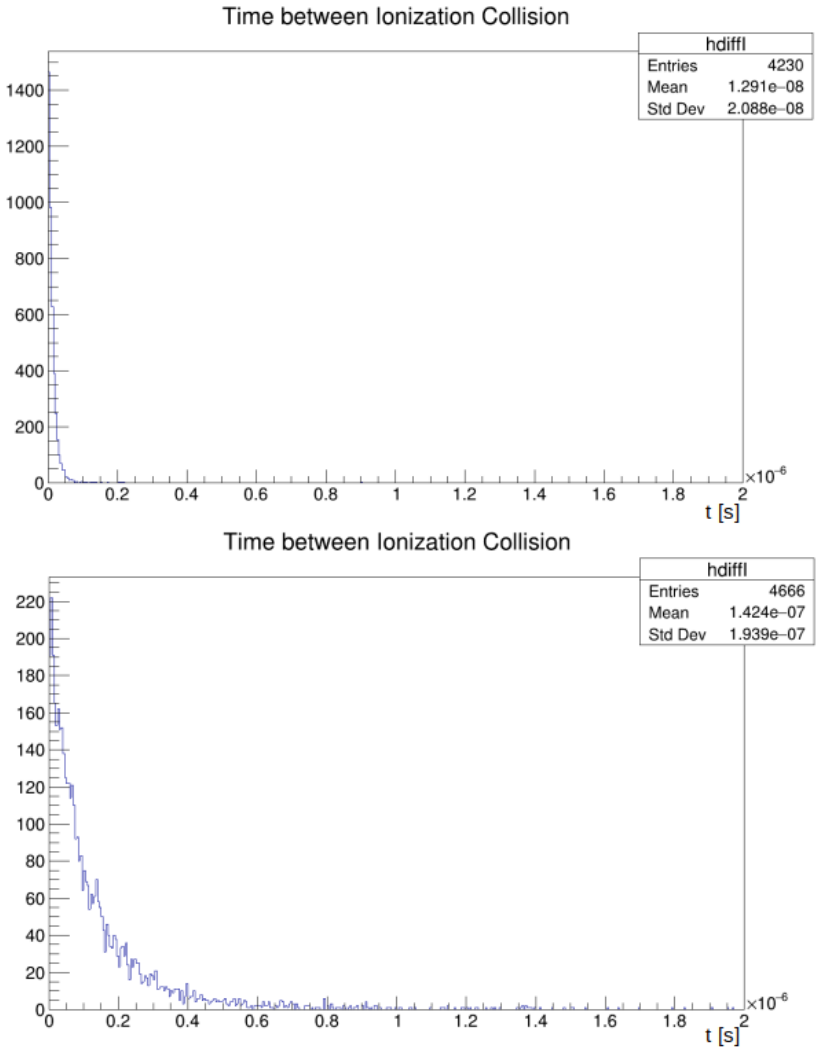


**Figure 4.31:** *Time differences between consecutive ionizations for 500 electrons at the pressure of $10^{-7}$ mbar (top) and for 1000 electrons at the pressure of $10^{-8}$ mbar (bottom)*

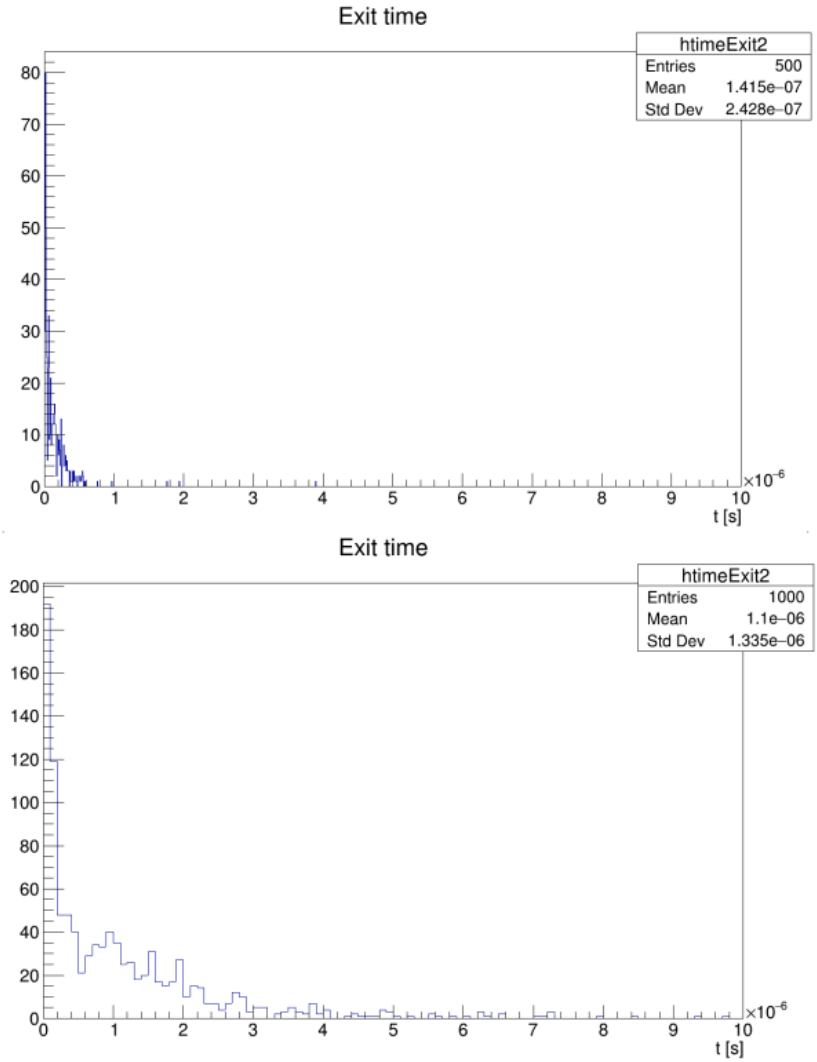


**Figure 4.32:** *Lifetimes of 500 electrons at the pressure of $10^{-7}$ mbar (top) and for 1000 electrons at the pressure of $10^{-8}$ mbar (bottom)*

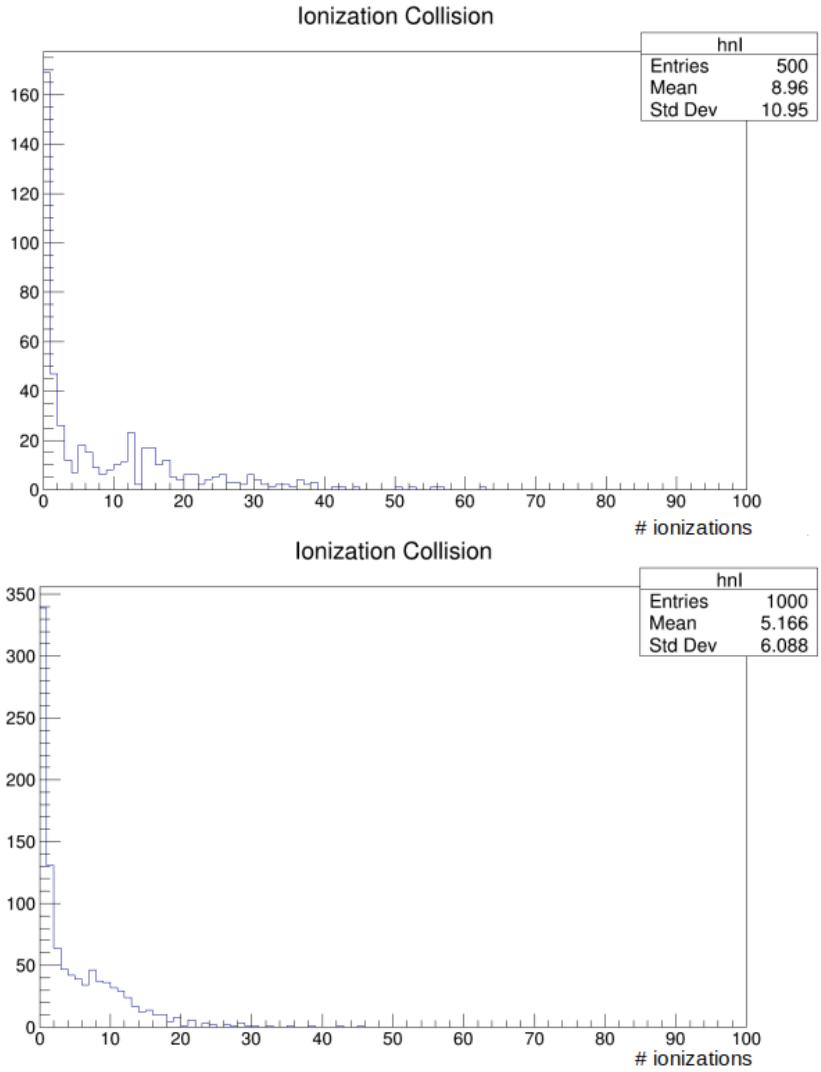


**Figure 4.33:** *Number of ionizations for each electron at the pressure of $10^{-7}$ mbar (top) obtained from 500 simulations and at the pressure of $10^{-8}$ mbar (bottom) obtained from 1000 simulations*

electrons change in time in order to calculate the ion current. Since the number of electrons inside the trap is very large (the order of magnitude is about $10^{10}$), it is not possible to simulate the trajectory of each electron, but from the distributions mentioned above, i.e. time between ionizations, total electron lifetime and number of ionizations during its life, random data are extracted. So, a first electron is generated near the cathode. A value is extracted from every distribution and assigned to it. After that a timer starts. When it reaches the ionization time assigned to the electron, an ionization takes place and an electron-ion pair is generated. The secondary electron is neglected in this first version of simulation because, as mentioned before, typically it is generated close the trap center, so with a low potential energy and with zero kinetic energy, i.e. unable to make multiple ionization. That is why they are considered to end up in the plasma. The ion is immediately accelerated towards one cathode where it emits an electron. For this electron another set of values of time of ionization, lifetime and number of ionizations are assigned as for the previous one. Meanwhile the ionization time of the first electron is updated and the number of possible ionizations is reduced by one. So for every time step and for every electron:

- total time is compared with ionization time;
- one more (secondary) electron is added if an ionization occurs;
- number of ions that collide with the cathode are counted

When the electron performs all possible ionizations or when it reaches its lifetime it is removed from the simulation. So number of ions that collide with the cathode are studied as a function of the total time in order to calculate the

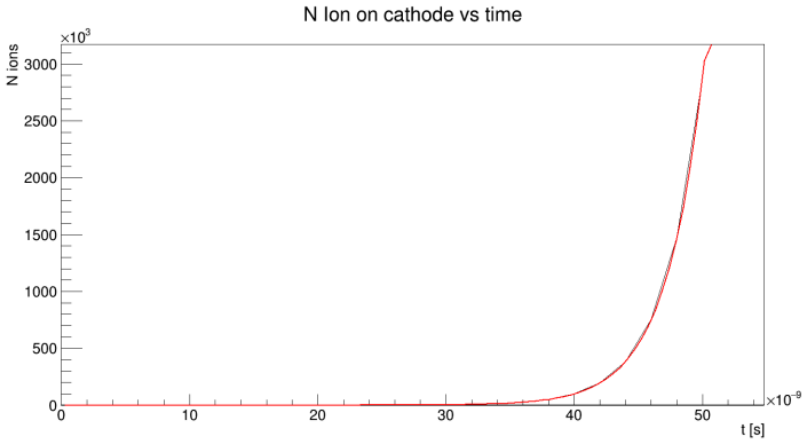


**Figure 4.34:** *Number of ions colliding with the cathode vs. time and exponential fitting function*

current at different pressures. Again, a full simulation of current vs pressure can not run because of the large number of electrons and ions involved. The approach used is to run the simulation up to the maximum number of ions which can be followed in a reasonable amount of time and then extrapolate the information needed. The number of ions produced N(t) vs time follow an exponential law:

$$N(t) = N_0 \cdot exp(p_1 t) \tag{4.4}$$

where $N_0$ is the number of initial electrons and $p_1$ is a function parameter (ionization frequency). Running an exponential fit on 1000 simulations at the same conditions allows to make an estimation of the ionization frequency as shown in Fig.4.34 and Fig.4.35.

At this point we are ready for the current and pumping speed calculation that we will show in the next chapter.

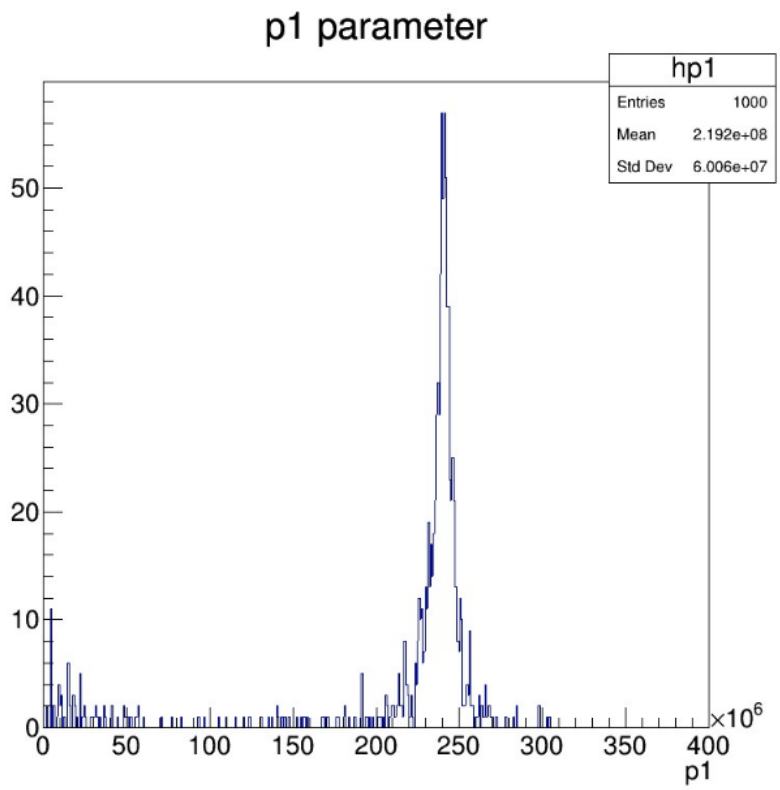


**Figure 4.35:** *Parameter $p_1$ of fitting function of number of ions vs time considering a pressure of $5 \cdot 10^{-1}$mbar (that will be re-scaled in $5 \cdot 10^{-7}$mbar)*

# Chapter 5

# Ion current and pumping speed simulations

The parametric simulation used in the previous chapter is used to built the ionization frequency distribution. This parameter is the one which allows us to calculate the current. Moreover we know that the maximum number of electrons $N_B$ is defined by the Brillouin limit and that the current depends from pressure, but since this last one changes in a time scale much larger than the phenomenon considered, we can calculate from time to time the current at constant pressure as:

$$I = qN_B\overline{p_1} \tag{5.1}$$

where $q$ is the elementary charge. This operation is repeated for the different pressures values in order to obtain the current-pressure curve. In these simulations a single cell powered by 3 $kV$ and with a magnetic field of 0.12 $T$ was considered. As background gas, $N_2$ or $H_2$ were used. The current is

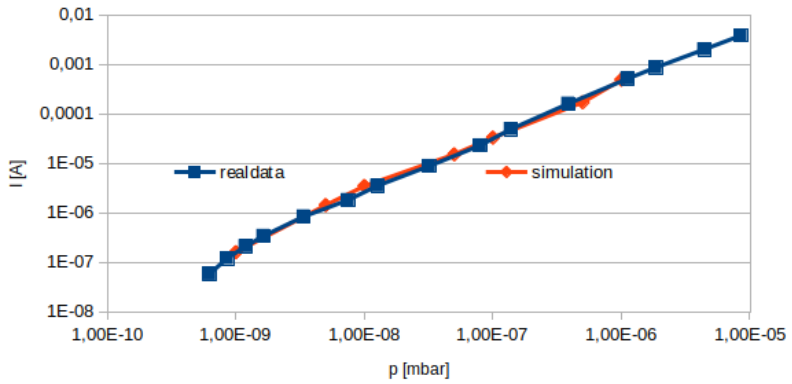


**Figure 5.1:** *Current-pressure curve obtained using $N_2$ as a buffer gas and considering a 40 l/s ion pump*

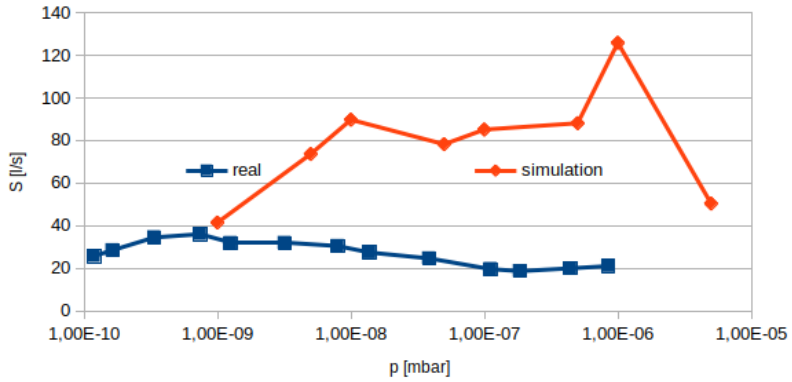


**Figure 5.2:** *Pumping speed obtained using $N_2$ as a buffer gas for a 40 l/s ion pump*

calculated for a single cell and then is multiplied by the number of cells in the ion pump.

A comparison with the experimental data is shown in Fig.5.1, where there is a good agreement between experimental and simulated data.

The last step is the calculation of the ionization pumping speed obtained as $S = k\frac{I}{P}$ (Eq.3.3). In Fig.5.2 the ionization pumping speed simulated is compared with the pumping speed measured from an Agilent Diode VIP 40 with $N_2$ as background gas.

It is clear that the simulation is completely different from the real data. That

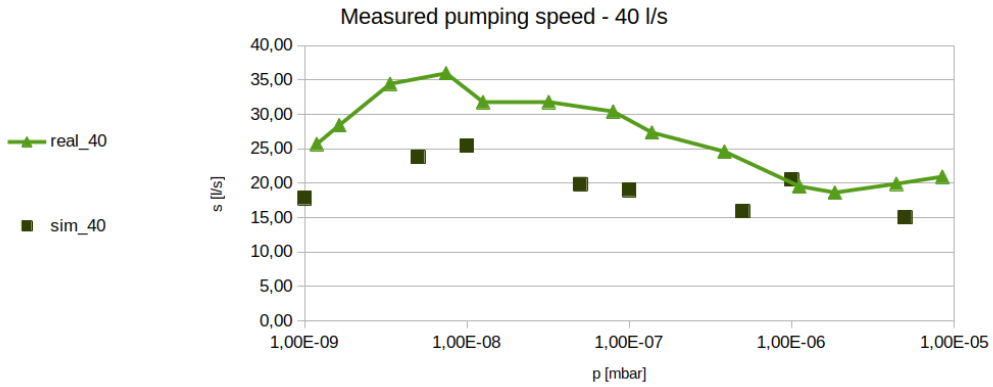


**Figure 5.3:** *MPS for a 40 l/s ion pump at 3 kV considering $N_2$ as background gas*

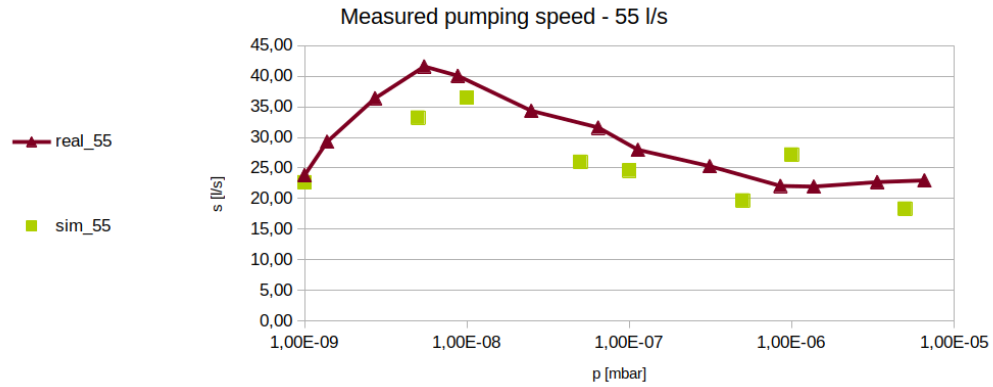


**Figure 5.4:** *MPS for a 55 l/s ion pump at 3 kV considering $N_2$ as background gas*

because, as explained in chapter 3, the measured pumping speed (represented by the real data) is different from the theoretical one (represented in this case by simulated data), as the influence of conductance, sputtering and sticking coefficient must still be taken into account (see Eq.3.4). By including these effects the measured pumping speed simulated has a better agreement with the real data, as shown in Fig.5.3.

The same comparison is done with the Agilent Diode VIP 55 and 75 (respectively in Fig.5.4 and Fig.5.5) which have the same characteristics of the Diode VIP 40, but a different conductance.

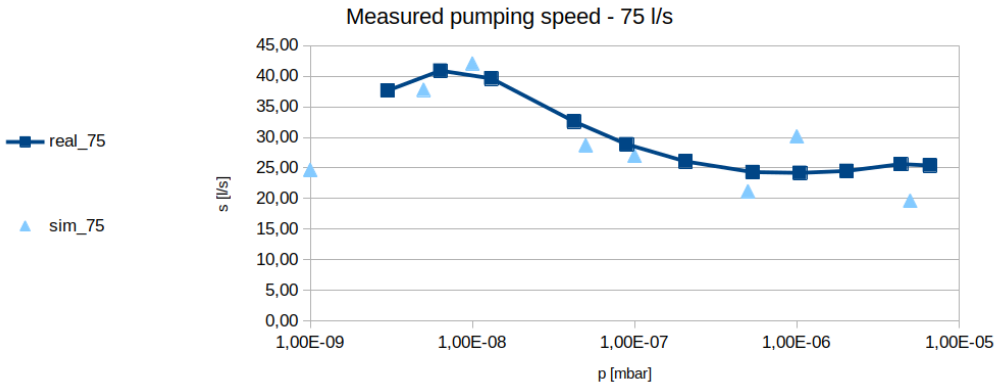


**Figure 5.5:** *MPS for a 75 l/s ion pump at 3 kV considering $N_2$ as background gas*

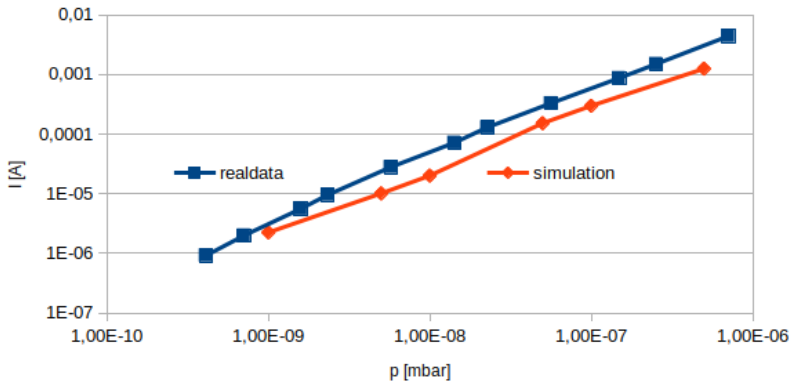


**Figure 5.6:** *Current-pressure curve obtained using $H_2$ as a buffer gas and considering a 800 l/s ion pump*

The simulation seems to be in good agreement with the real data for the Diode VIP 55 and 75 supplied by 3 *kV*. An error of about 20% can be observed for the Diode VIP 40. This discrepancy could arise from the calculation of the conductance, as it is the only part that differs from the Diode VIP 55 and 75. Other simulations were done taking into account as background gas $H_2$ instead of $N_2$. In this case a 800 *l/s* ion pump is considered, obtaining the current simulation as in Fig.5.6.

The difference between the real and simulated data is considerable in this case. That is due to the fact that the pump simulated has much larger

dimensions (i.e. more Penning cells) with respect the Diode VIP 40, 55 and 75. The approximation by which the current is calculated for a single cell is multiplied by the total number of cells reduces its effectiveness for larger pumps with many cells. Furthermore hydrogen has very different properties with respect to nitrogen: its diffusion into the Titanium cathode is not considered nor the probability to be desorbed which affect the current and pumping speed [47]. All these studies concerning particular properties of single gases will have to be studied and implemented individually in the future.

## 5.1 Current and pumping speed considering different operating parameters

Simulations of some ion pumps using standard parameters ($U_0 = 3\ kV$, B = $0.12\ T$, $r_{anode} = 10\ mm$) gave good results using $N_2$ as background gas. So the next step is to understand if this pump model is still a good approximation when using different operating parameters. If this proves true it would be an excellent result as it would allow the simulation to be used to test different types of ion pumps. Only $N_2$ is used as background gas in these simulations as with this gas the best results were obtained.

For some of these data the uncertainties were calculated. At the moment it has not yet possible to calculate them for all the curves simulated, as we will explain shortly, the uncertainties calculation requires a much larger number of trajectories simulations (at least 5 times greater than the number

of simulations considered so far). It is not possible to proceed with the propagation of errors as it is difficult to associate an uncertainty to the various parameters used for the current calculation. But since each event simulated is independent from the others and the calculated current value is subject to the statistical fluctuations, we can obtain the current value at the same pressure multiple times, starting from different trajectory simulations; the uncertainty will be the difference between the maximum and minimum current value calculated. This requires more trajectories simulations: in particular, we have empirically considered the need to increase them by 5 times (for pressure higher than $10^{-7}$ *mbar* 500 simulations of the same event are needed when the error is not calculated and 2500 simulations are needed when the error is calculated; for the lower ones 1000 simulations of the same event are needed when the error is not calculated and 5000 are needed when the error is calculated). Then we created 10 groups of 500 simulations each (or 1000 simulations each for pressure lower than $10^{-7}$ *mbar*), randomly extracted from the (2500 or 5000) total. We have calculated the parameters distributions and the the current for every group of simulations and finally the maximum deviation. The "real" value calculated at a certain pressure is obtained taking into account all the 2500 or 5000 simulations.

### 5.1.1 Different supply voltages

The first tests to verify the robustness of the simulation are done considering different supply voltages without changing the other boundary conditions. Presently only the I/P ratios is calculated, because at the moment we have

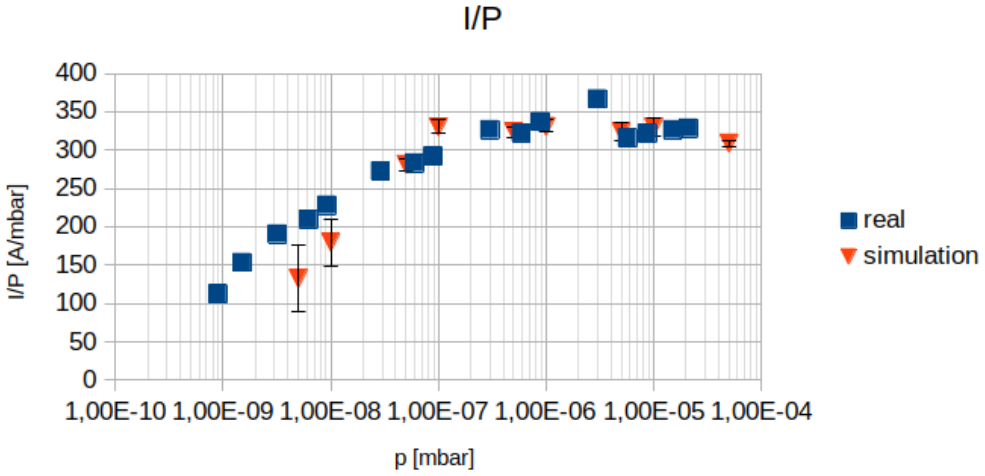


**Figure 5.7:** *I/P ratio for an ion pump supplied by 5 kV of voltage*

not real pumping speed data in the conditions we are studying. To obtain them it would be necessary to reconstitute a new experimental set to collect new data. But as explained before, this ratio is extremely useful to obtain the pumping speed and this is sufficient to understand if the simulation is working well. So in Fig.5.7 and Fig.5.8 are reported respectively the I/P ratio at different pressures for ion pumps supplied by 5 $kV$ and 7 $kV$ and with a magnetic field of 0.12 $T$.

Simulations using different voltage at cathodes seem to be in a good agreement with the real data.

### 5.1.2 Different magnetic field

The next step is to understand if simulation responds well to different magnetic field values. This comparison has been done considering a power supply at 7 $kV$. So in Fig.5.9, Fig.5.10 and Fig.5.11 are reported respectively the I/P ratios for ion pumps with a magnetic field of 0.14 $T$, 0.16 $T$ and 0.22 $T$.

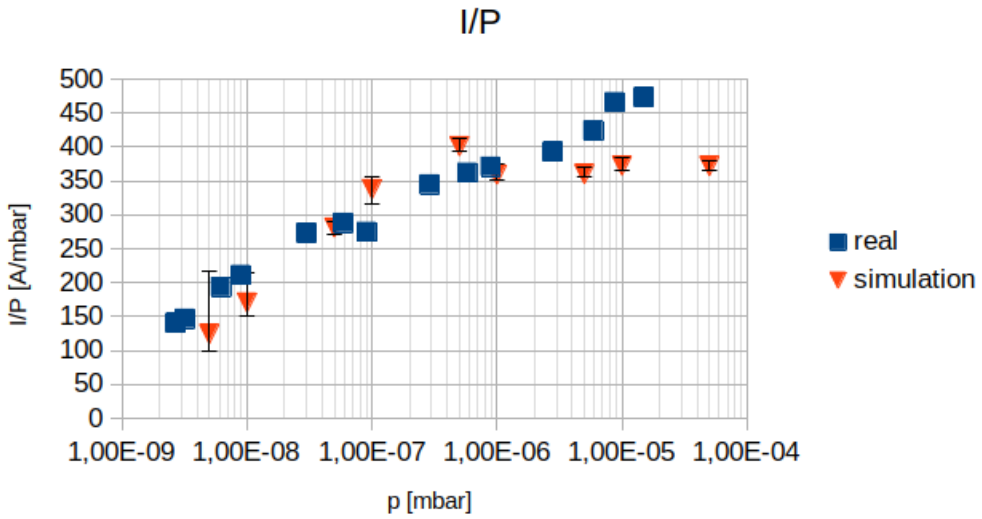


**Figure 5.8:** *I/P ratio for an ion pump supplied by 7 kV of voltage*

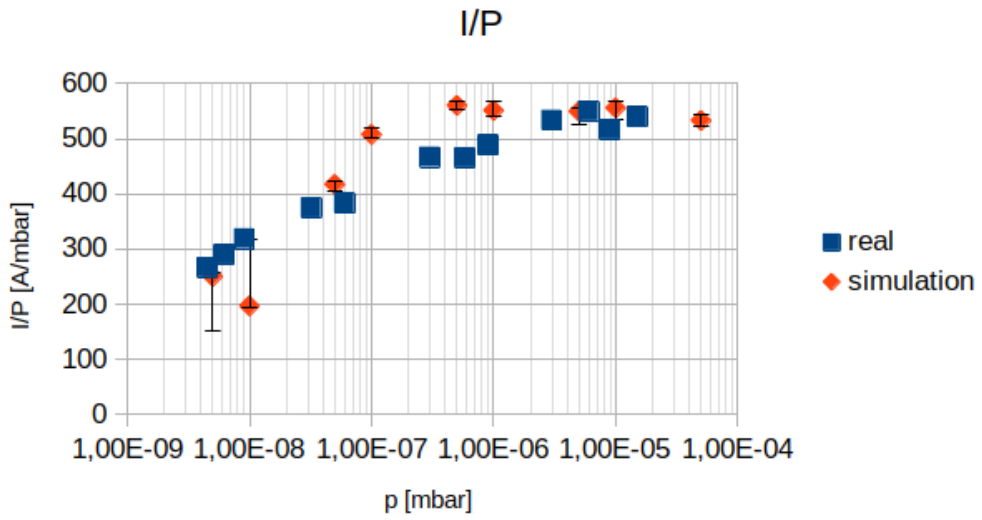


**Figure 5.9:** *I/P ratio for an ion pump supplied by 7 kV of voltage and with a magnetic field of 0.14 T*

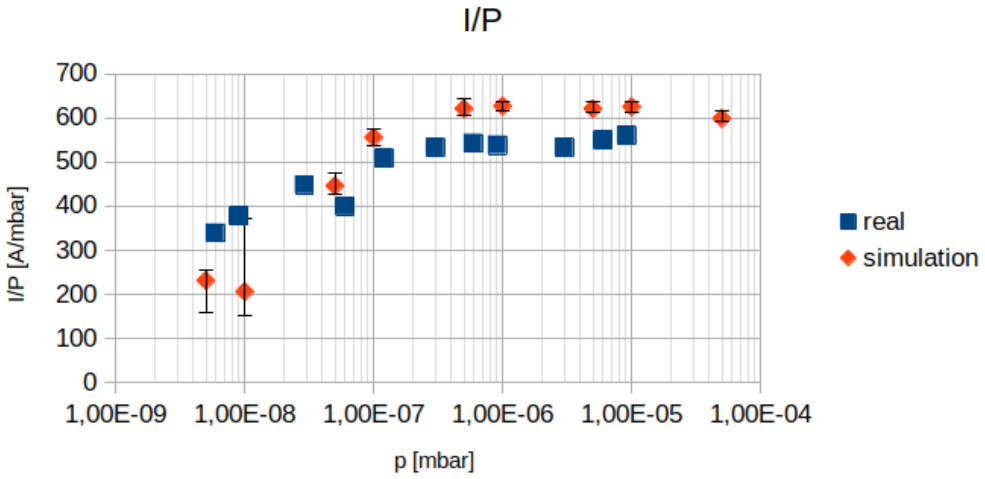


**Figure 5.10:** *I/P ratio for an ion pump supplied by 7 kV of voltage and with a magnetic field of 0.16 T*

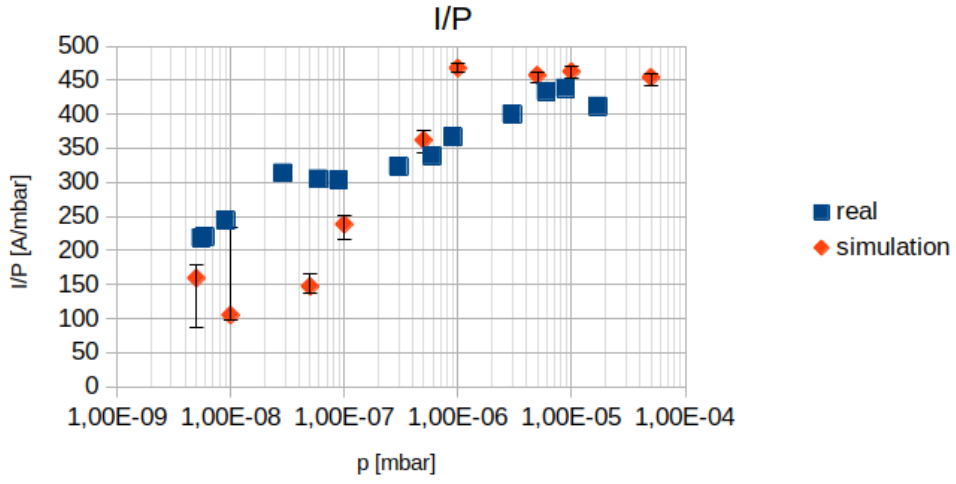


**Figure 5.11:** *I/P ratio for an ion pump supplied by 7 kV of voltage and with a magnetic field of 0.22 T*

The simulation using a magnetic field of 0.16 *T* seems to be in good agreement with the real data. For the case with 0.14 *T* we have a good agreement at low pressures (P<$10^{-7}$ mbar) but not for the higher pressures. It is still not very clear why this happens and what the cause is, especially taking into account that in the experimental data one would expect to see a decrease in the growth of I/P values for pressures grater than $10^{-6}$ mbar as happens in the other curves and in simulated data. Therefore it cannot be excluded that there may have been problems in taking real data. At the moment, however, this does not worry us that much because we are more interested in having a good simulation for low pressures and this seems to happen with a good agreement. The worst curve is the one where we used a magnetic field of 0.22 *T*. In that case if we take into account the I/P values and their error we have the general trend vaguely similar with the real one except for two values (at pressures of $5 \cdot 10^{-8}$ mbar and $10^{-6}$ mbar). This problem is also encountered in other simulations where sometimes a certain point (not always at the same pressure) is completely different from the real data. At this moment it is not really clear why this happens: the most probable causes, however, could be related either to a low statistic used to build the parameters distributions or to a bad binning of these distributions. Moreover, the intensity of the magnetic field considered is such that the behavior of the plasma could be different from what we have considered up to now as we will see in 5.3. Other studies should be done in order to understand the causes of the problem.

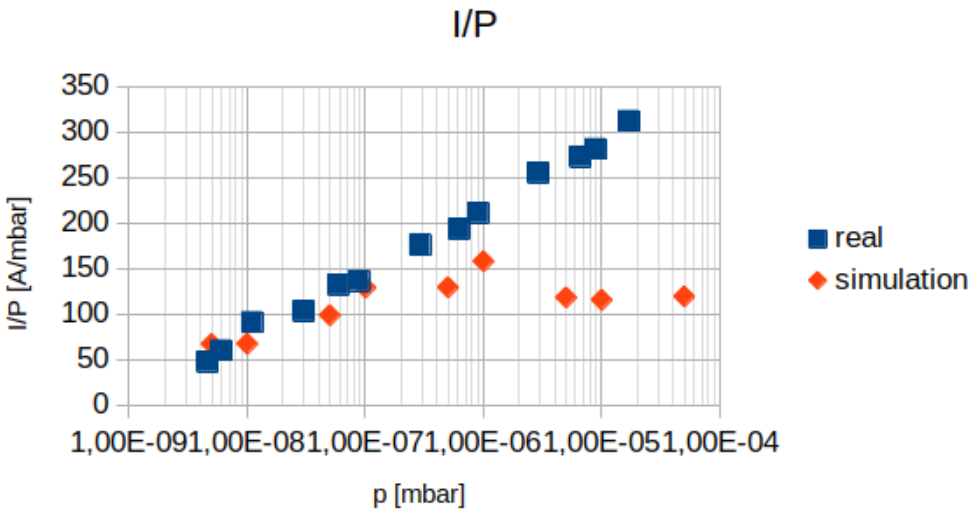


**Figure 5.12:** *I/P ratio for an ion pump with a radius of the anode of 6 mm supplied by 5 kV of voltage and with a magnetic field of 0.14 T*

### 5.1.3 Different radius of the anode

The last parameter that we changed to understand the reliability of the simulation is the radius of the anode. The results are reported in Fig.5.12, Fig.5.13, Fig.5.14, Fig.5.15, Fig.5.16. For these data the error has not been calculated, as it would take too long to do all the required simulations.

Observing the curves it seems that simulated data are in an acceptable agreement with the real data for pressures lower than $10^{-6}$ *mbar* but with a different trend for higher pressures. Also in this case other studies should be done in order to understand if there is a problem in simulations or in the real measures. This last hypothesis is taken into account because in these cases the I/P trend seems to increase indefinitely with increasing pressures, while, as seen before, normally this ratio tends to stabilize at higher pressures.

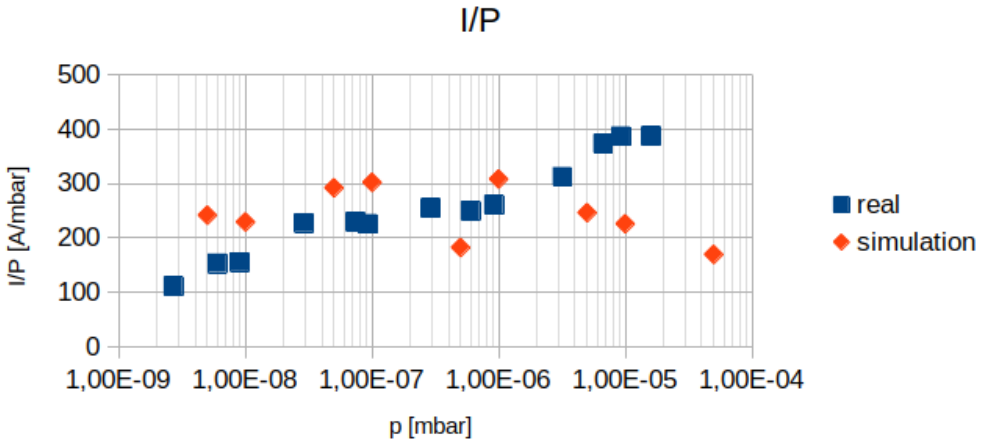


**Figure 5.13:** *I/P ratio for an ion pump with a radius of the anode of 7 mm supplied by 5 kV of voltage and with a magnetic field of 0.14 T*

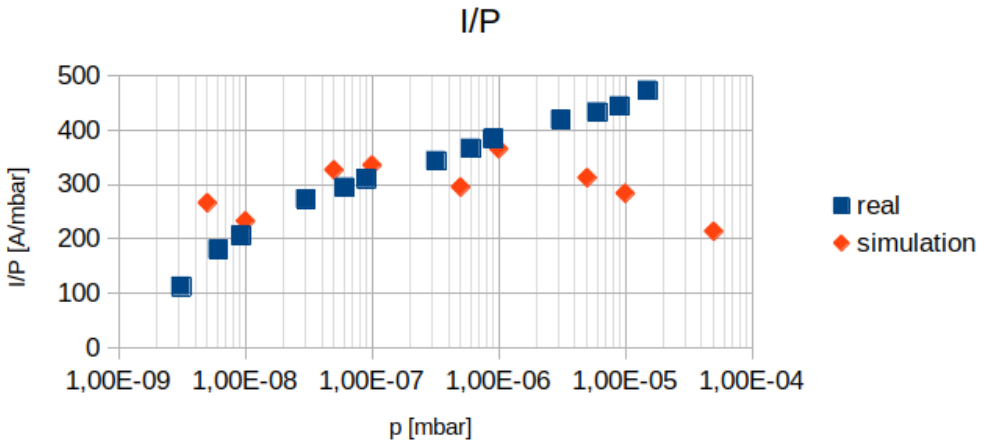


**Figure 5.14:** *I/P ratio for an ion pump with a radius of the anode of 8 mm supplied by 5 kV of voltage and with a magnetic field of 0.14 T*

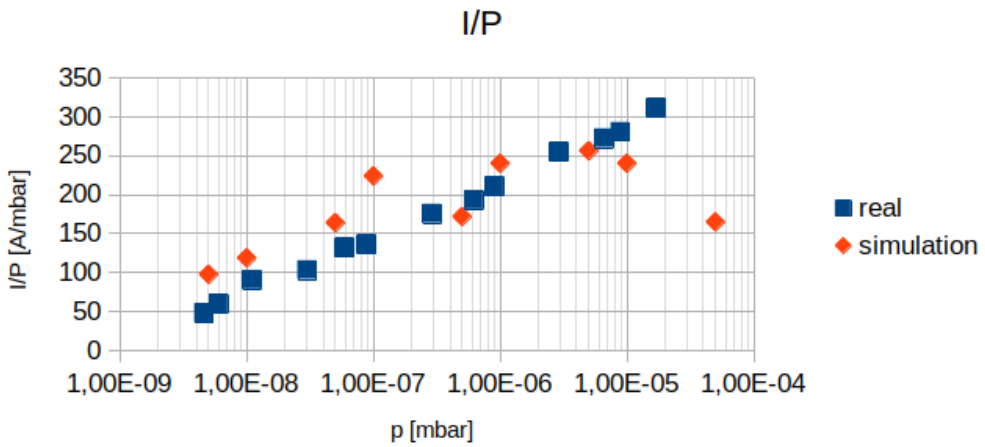


**Figure 5.15:** *I/P ratio for an ion pump with a radius of the anode of 12 mm supplied by 5 kV of voltage and with a magnetic field of 0.14 T*

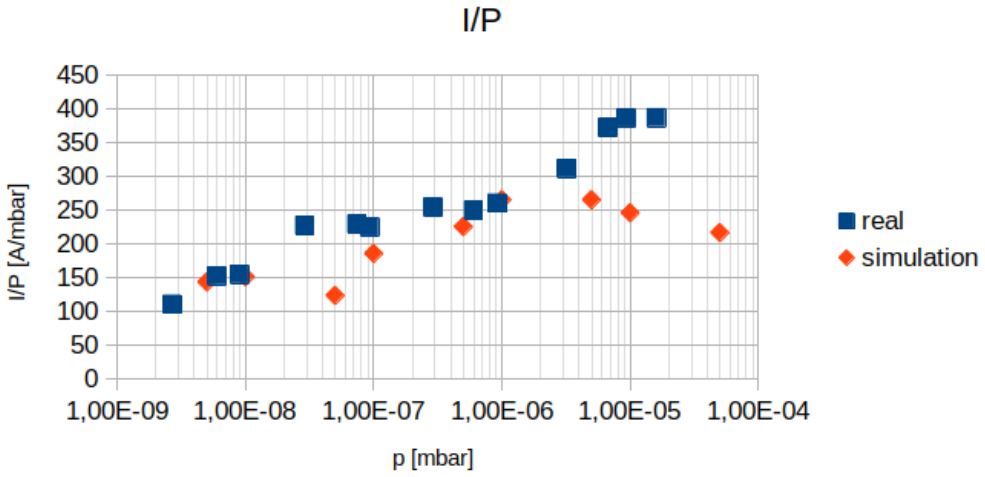


**Figure 5.16:** *I/P ratio for an ion pump with a radius of the anode of 14 mm supplied by 5 kV of voltage and with a magnetic field of 0.14 T*

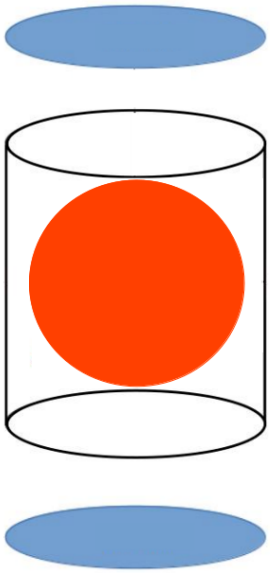

**Figure 5.17:** *Example of spherical plasma (red) used in simulations*

## 5.2 Studies on plasma shape

As explained in 4.5, simulations consider a cylindrical plasma with the same radius of the anode cell and with 4 *mm* of height, but most likely it is not the real plasma shape. So, different simulations were done considering different plasma shapes (spherical and prolate spheroidal as in Fig.5.17 and Fig.5.18) with the same volume, in order to understand its influence on current (and pumping speed) data. All the plasma shapes have the center coincident with that of the trap.

Current-pressure ratios obtained are shown in Fig.5.19 and in Fig.5.20 where the plasma considered has respectively a spherical and ellipsoidal shape.

Observing these two simulations it seems that both of them are a good approximation of the real data as well as the one obtained with a cylindrical plasma. This results show that the plasma shape does not have a strong influence on the current value (and therefore on the pumping speed). The

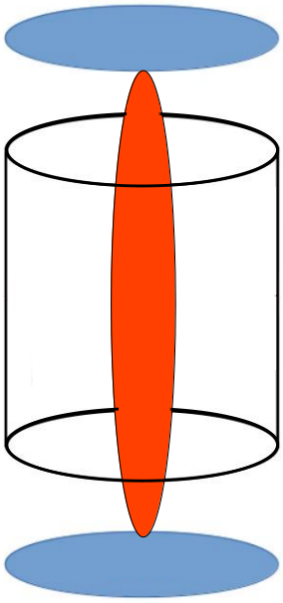

**Figure 5.18:** *Example of prolate spheroidal electron plasma (red) used in simulations*

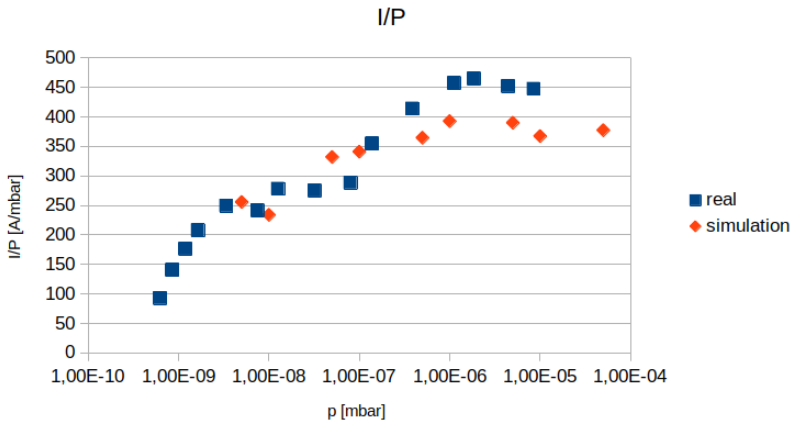


**Figure 5.19:** *I/P ratio for an ion pump with a radius of the anode of 10 mm supplied by 3 kV of voltage and with a magnetic field of 0.12 T considering a spherical plasma with 8 mm of radius*

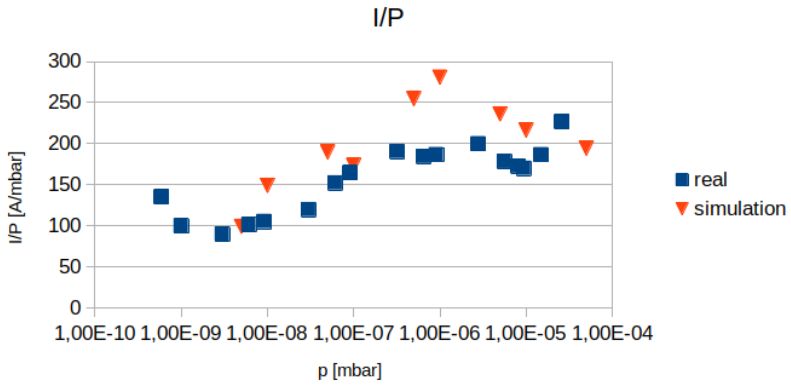


**Figure 5.20:** *I/P ratio for an ion pump with a radius of the anode of 10 mm supplied by 3 kV of voltage and with a magnetic field of 0.12 T considering an ellipsoidal plasma with 6 mm of radius and an height equal to the distance between the cathodes*

important parameter which we have to know is the portion of the total volume that the electron cloud occupies (i.e. the plasma volume).

## 5.3 Studies on ion pump design

Other studies on ion pump design were done in order to understand which parameters configuration generates a better performance. This study is not innovative in that it follows Schuurman's and Hartwig's studies [18, 43] and Paolini's measurements [36], but it is done to understand if through simulation it is possible to obtain data comparable with reality. In particular it was verified the transition from the Low Magnetic Field (LMF) to the High Magnetic Field (HMF) when the parameters change (anode diameter and supply voltage). We will not make a theoretical discussion of the two modes, but we'll just report the Schurmann's description where the low mode "*is based on Poisson's equation and the continuity equation for electrons*", while

the high mode "*is only valid in a small stable region of the discharge*". A more detailed description of the difference between the two modes can be found in his studies.

The magnetic field transition ($B_t$) is obtained from Hartwig as:

$$B_t = \frac{7.63 \cdot \sqrt{U_0}}{r P^{0.05}} \tag{5.2}$$

where $B_t$ is expressed in *Gauss*, $U_0$ is expressed in *Volts*, *P* is the pressure expressed in *Torr* and *r* is the radius expressed in *cm*. These tests are done considering always the same pressure that is $10^{-7}$ *mbar*, since ion pumps are typically used at this pressure value. At this point the trend of the current can be extracted for different values of magnetic field in a range between 1000 *G* and 2200 *G*. This trend is calculated both by keeping the dimensions of the anode constant and varying the supply voltages and vice versa. as shown respectively in Fig.5.21 and Fig.5.22.

In all cases the current increases as the magnetic field increases until the transition point is reached, then it begins to decrease. The goal of this analysis would be to understand if the simulation can predict the transition point or not. To this end, different trends are fitted with a second degree polynomial in order to calculate the maximum of the function. After that, all the transition points are compared with the theoretical trend (reported in Eq.5.2) as shown in Fig.5.23 and Fig.5.24.

Simulated data obtained have not the same absolute values theoretically predicted, but they have a quite similar trend. Unfortunately, this is not always true for all analysis, as some of them appear to have trends that

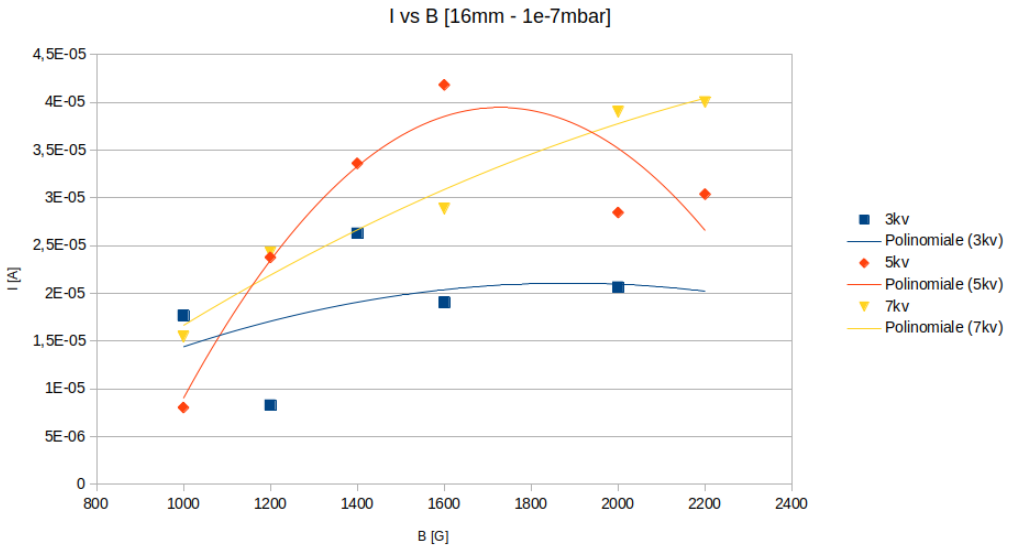


**Figure 5.21:** *Current vs magnetic field considering ion pumps with anodes of 8 mm radius each*

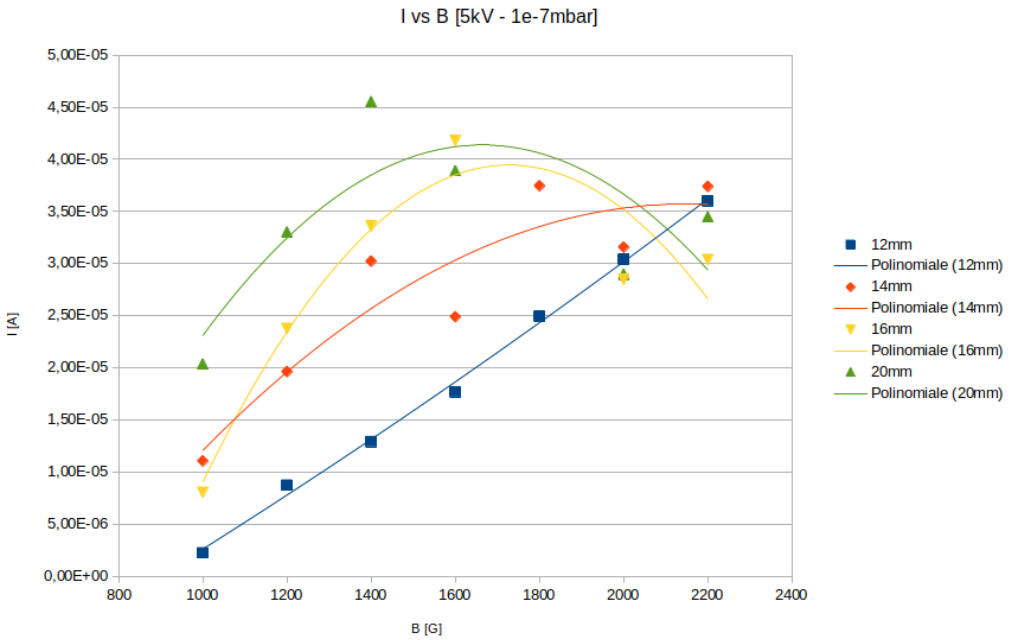


**Figure 5.22:** *Current vs magnetic field considering ion pumps supplied by 5 kV*

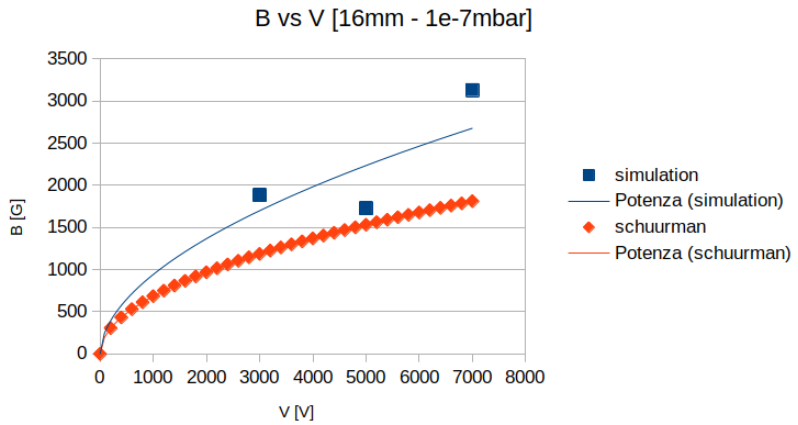


**Figure 5.23:** *Magnetic transition points at different ion pumps supply voltages compared with the theoretical trend (keeping constant the radius of anodes at 8 mm)*

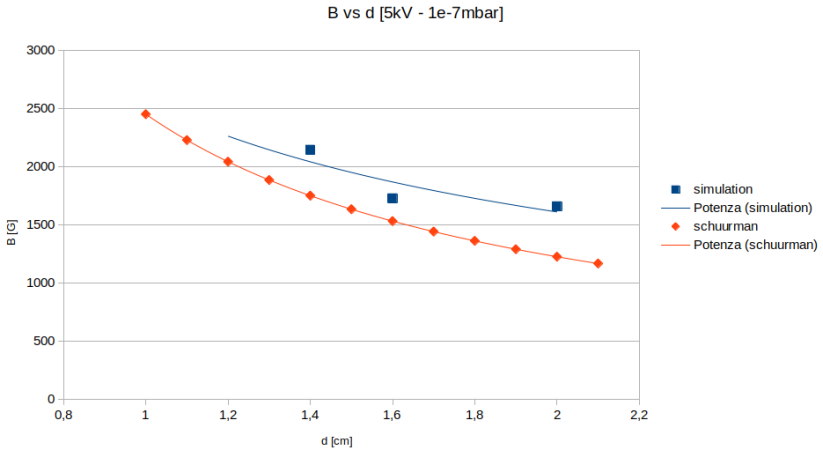


**Figure 5.24:** *Magnetic transition points at different ion pumps diameters of anodes compared with the theoretical trend (keeping constant the supply voltage at 5 kV)*

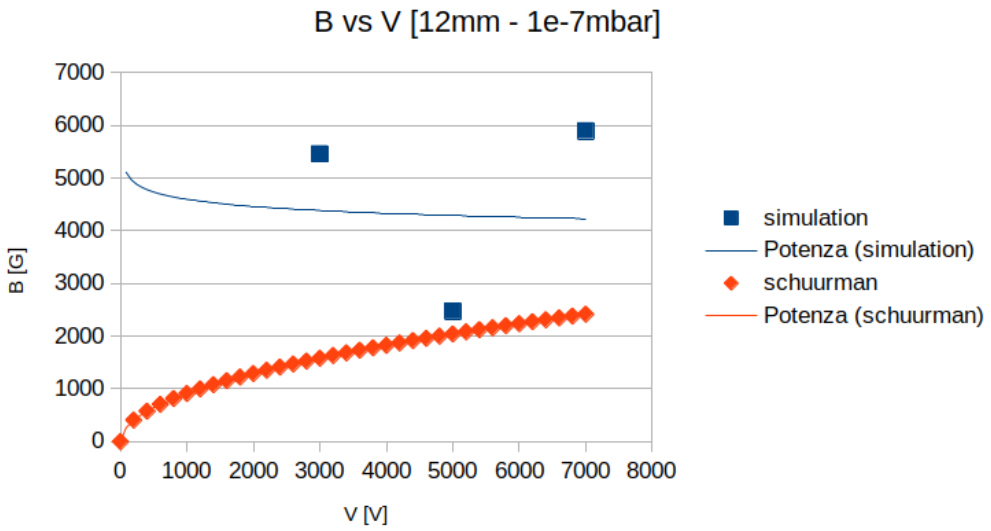


**Figure 5.25:** *Magnetic transition points at different ion pumps supply voltages compared with the theoretical trend (keeping constant the radius of anodes at 6 mm)*

are much more distant from what was predicted as shown in Fig.5.25 and Fig.5.26

From that figures is clear that the trends are quite different with respect to the theoretical ones. This can depend on several factors: the first one is that there are few points that can be used to build the trends and this can lead to have curves completely different from those theorized (as in Fig.5.25); moreover, the error on a single point leads to a large error on the fit (Fig.5.26). Moreover, all these analysis are done considering a certain pressure value ($10^{-7}$ *mbar*): it would be interesting to see what happen considering lower pressures. Furthermore, as the transition values are calculated considering the currents obtained from different configurations of the ion pumps, it is sufficient that one of those points has a greater error, for example because of low statistics, to obtain bad polynomial fits which influence considerably the

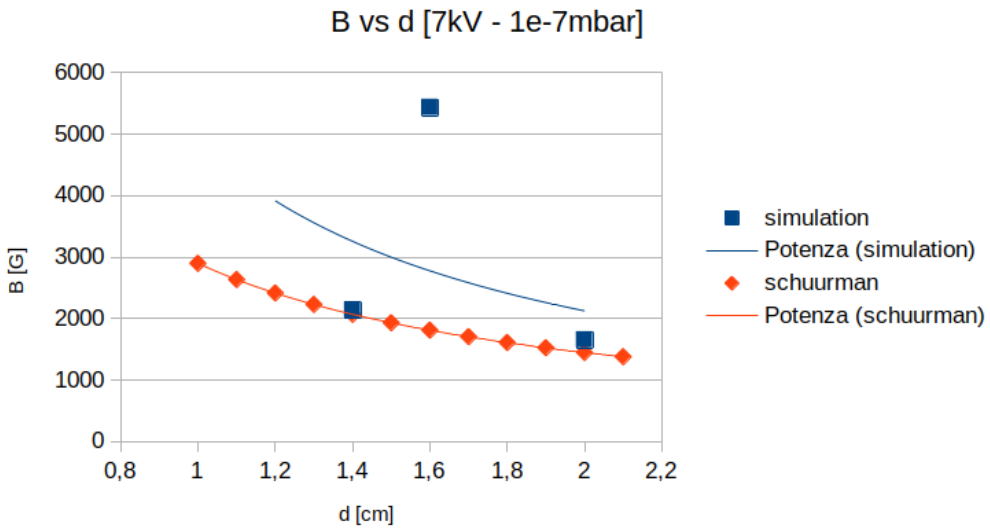


**Figure 5.26:** *Magnetic transition points at different ion pumps diameters of anodes compared with the theoretical trend (keeping constant the supply voltage at 7 kV)*

transition value. In the end, a better analysis could be done by considering the electron cloud as a sheath around the anode for magnetic fields greater than the transition value (HMF) as explained in [43].

## 5.4 GUI to launch multiple simulations

As explained before, this model used to calculate the ion pump performances is based on multiple simulations of a single electron with different background gas pressures. So, in order to optimize simulation times, a script is written that automates the process of consecutive simulations at different pressures, supply voltages, anode dimension and magnetic field. In principle all these parameters have to be changed in a text file which is read by the simulation algorithm and that executes the instructions given by the user. But in order

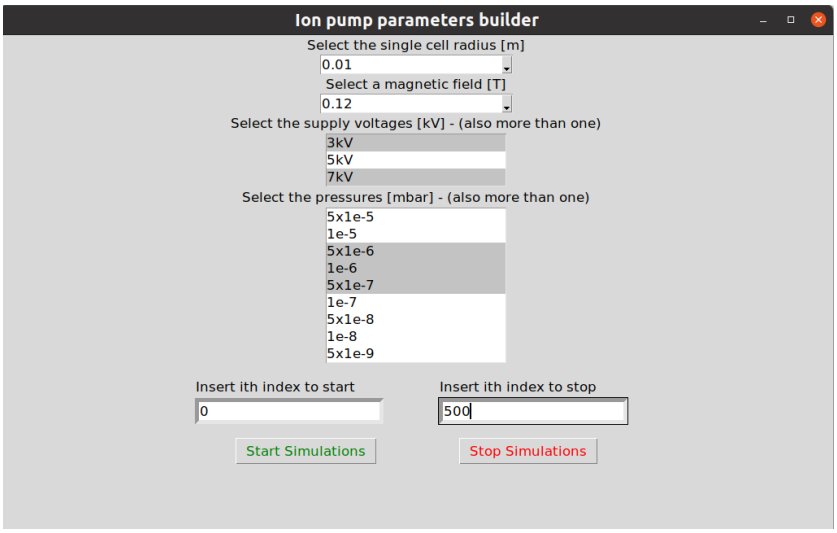


**Figure 5.27:** *Graphical interface to manage and launch consecutive simulations using different operating parameters of the ion pump*

to simplify the parameters modification operations a GUI is written. It is used the *Tkinter listbox* widget of Python to implement it. Graphical interface is really simple and it is shown in Fig.5.27.

First two lines allow to the user to select from two different drop-down menus respectively the radius of the anode expressed in *meters* and the intensity of the axial magnetic field expressed in *Tesla*. In third line users can choose the supply voltage at the cathode. These voltages are expressed in absolute value, but in simulation are considered as negative. More than one voltage can be selected: for example in Fig.5.27 the algorithm is set to simulate ion pumps supplied by 3 *kV* and 7 *kV*. Fourth line allows to the user to select the pressures of the background gas expressed in *mbar*. In that section it is also possible to select more than one pressure: in this example the pressures $5 \cdot 10^{-6}, 10^{-6}$ and $5 \cdot 10^{-7}$ *mbar* are selected. The last line allows to the user to choose how many repeated simulations have to be done for each pressure by choosing the initial and final index with which simulations are numbered.

User has to remember that for pressures equal or lower than $5 \cdot 10^{-8}$ *mbar* the final index is multiplied by 2 in order to increment the statistics. In this example all simulations at a certain pressure start with the index *0* but:

- to simulate pressures higher than $5 \cdot 10^{-8}$ *mbar*, 500 repeated simulations are done for each pressure value;
- to simulate pressures equal or lower than $5 \cdot 10^{-8}$ *mbar*, 1000 ($500 \cdot 2$) repeated simulations are done for each pressure value.

Then, when all parameters are set, user can start the simulations clicking on *Start Simulations* and stop them clicking on *Stop Simulations*. Up to now the path of the simulations can be modified only within the script text file, but once the source folder has been decided, all the internal folders that sort and divide the simulations based on the chosen parameters are produced automatically. In particular, simulations are produced consecutively in loops: the cycles on the parameters go from the most external to the most internal following the order in which they are presented in the GUI. So the algorithm produce simulations in the following way:

- the radius of the anode and the magnetic field are selected and they will never change during the loops;
- voltage and pressure are fixed. The first voltage considered is that one with the lowest value and the first pressure considered is the one with the highest value selected from the menus. Then a certain number of simulations from the initial and final indexes are produced;
- keeping the voltage fixed, another set of simulations (following the index numbers entered) are done considering the next lower pressure

selected from the menu;

- when all pressures at a certain voltage are simulated, the next higher voltage selected from the menu is simulated.

All this can be resumed with the scheme in Fig.5.28.

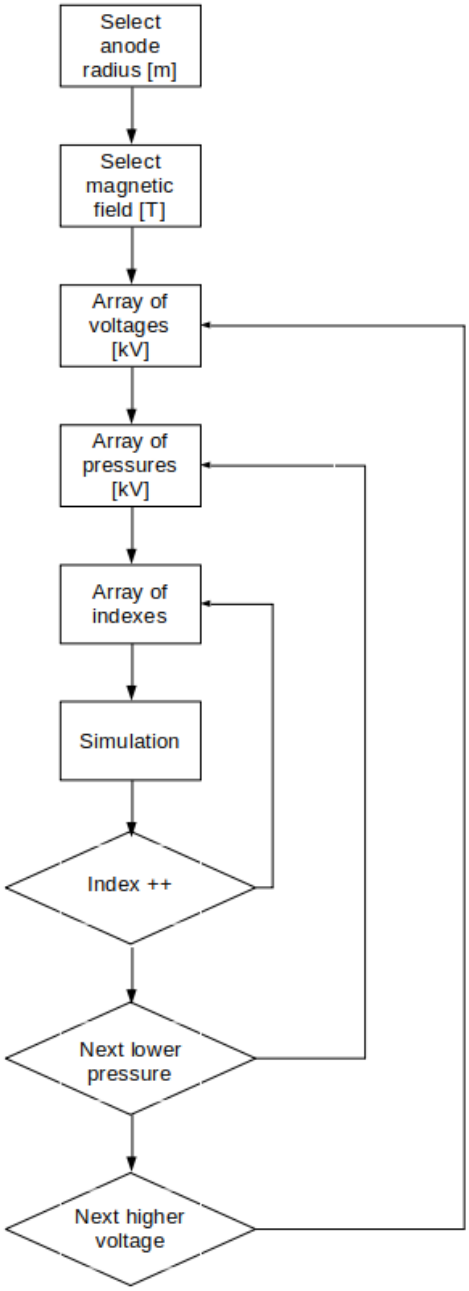


**Figure 5.28:** *Block diagram describing the order of the simulations*

# Chapter 6

# Summary and conclusions

The aim of this work consists in studying and implementing a mathematical model to simulate the performances of the sputter ion pumps (SIP), which work at pressures between $10^{-5}mbar$ and $10^{-10}mbar$. They are capture vacuum pumps which operate by sputtering a getter material. The main element of the ion pump is the Penning cell, i.e. a device which is able to trap electrons using a quadrupolar electric field and an axial magnetic field. This fields are generated thanks to a cylindrical anode placed between two Titanium cathodes and two permanent magnets. Trapped electrons have sufficient energy to make multiple ionizations of the neutral background gas molecules. The electric field accelerates the ions toward one of the cathodes. The ion-cathode collisions sputter Titanium molecules which generate a chemical active film on anode. The main pumping consists in the neutral molecules that attach to that film and are buried in the anode. So, it is clear that the pumping speed (i.e. the quantity of gas moved out in the unit of time) is proportional to the current value. Since the current depends on the number

of ionizations which occurs inside the trap, we studied the parameters which influence them.

To do that we decided to simulate and sample step by step the entire trajectory of single electrons for a certain time in a trap with a background gas at a certain pressure. Since the number of electrons in the trap is too high to be able to simulate all their trajectories, we mapped in space and in time ionizations in order to create some parameters distributions (number of ionizations for each electron, life time and the time between consecutive ionizations). These distributions were used to calculate the number of ionizations for a large number of electrons (about $10^{10}$) without simulate all their trajectories and calculate the current and pumping speed.

In particular our work started using Simbuca, a tool able to simulate the electron trajectory in a Penning trap taking into account the presence of a background gas. It considers also the elastic collisions between electron and neutral molecules. After checking that it could be adapted to our purposes we studied the physics of the trap and then we implemented the other effects we need, such as the calculation of ionizations and inelastic collisions probabilities, the calculation of the scatter deviation taking into account the differential cross-sections and the loss of energy after interactions. After this first step we were able to verify the theoretical behavior of the electrons as the tendency of the magnetron radius to increase and of the axial oscillation to decrease when the electron looses energy or the dependency of its axial oscillation amplitude from its total energy. Furthermore, we understood from literature that after few milliseconds, in the trap an electron plasma due to the multiple ionizations is generated. This plasma influences the electric

field which acts on the electrons. The density of this non-neutral plasma is limited by the *Brillouin limit*, so we have implemented its influence on the electrons in Simbuca. The tricky part was to take into account the shape of the plasma: considering the volume inside the trap occupied by the electrons that have not enough energy to ionize, we decided to consider as cylindrical. Influence of plasma is implemented in Simbuca by passing to it the modified electromagnetic field (i.e. with the presence of plasma) calculated by using OpenFoam, a computational fluid dynamics (CFD) software. At this point the last implementation in Simbuca was the calculation of the collisions probabilities and the scattering angles in the interactions between the simulated electron and the plasma.

After obtaining an electron trajectory simulator which considers all the possible relevant phenomena, we proceeded with the building of the parameters distributions. They are obtained through repeated simulations of a single electron trajectory generated near the cathode with a background gas ($N_2$ or $H_2$) at a certain pressure. The choice to generate the electrons at the cathode was made because they contribute most to the number of ionizations as they have the greatest possible energy. The secondary electrons generated during ionizations were neglected in this first version of simulation because, in general, they are generated with a low energy, i.e. with a low capacity to make multiple ionizations.

The parameters distributions are obtained for every discrete value of pressure at which we want to know the current making 500 simulations of a single electrons for pressures equal or higher than $5 \cdot 10^{-7} mbar$ and 1000 for pressures lower than $5 \cdot 10^{-7} mbar$. The distributions obtained are the number of

ionizations that each electron does during its life, their life time i.e. the time which passes between the creation of the electron and its interaction with the trap wall or when it has not energy sufficient to ionize, the time between two consecutive ionizations. We used these distributions to build a parametric simulation. This one is able to calculate the number of ionizations for a large number of electrons as we did not need to simulate all their trajectories, but it was sufficient to randomly extract the values from the distributions built from us. From these simulations we extract the ionization frequency $p_1$ of the electrons at a certain background gas pressure and we use it to calculate the current *I* and the ionization pumping speed *S* as:

$$I = qN_B p_1$$

$$S = k\frac{I}{P}$$

The ionization pumping speed is a good parameter for describing the performance of the pump, but it is still not what we need as the pumping speed measured is influenced by the conductance, the sputtering yield and the sticking coefficient. We were able to calculate all these parameters respectively thanks to the Langmuir isotherm model, the semi-empirical Matsunami's formula and the work of Santeler. At this point we calculated the measured pumping speed $S_{eff}$ referred to a single Penning cell as:

$$S_{eff} = (\frac{1}{SC \cdot S'} + \frac{1}{C})^{-1}$$

where *S'* is the ionization pumping speed taking into account the conductance

due to the gap between anode and cathodes, *SC* is the sticking coefficient and *C* is the conductance of the connection tube between the pump and the vessel.

At this point, after multiplying this value for the number of Penning cell of the pump we had compared the simulations with the real data. The experimental data used to validate our model were taken from the Agilent Diode VIP 40, 55 and 75. The results of these comparisons suggested us that considering $N_2$ as background gas, the model seems to be in a good agreement with reality, in particular for the Diode VIP 55 and 75. An error of about 20% is committed for the Diode VIP 40 probably deriving from the calculation of the conductance, which is the only parameter that differs from the other pumps. Satisfactory results, however, were not obtained using $H_2$ as background gas. This because we have not taken into account the diffusion of the gas inside the cathodes and because we had experimental data for big SIP which has more Penning cells with respect to the Diode VIP 40, 55 and 75. Therefore all the approximations that have been made on the single cell are multiplied by a greater number, reducing the accuracy of the value obtained.

Finally we verified if our simulation could be used to predict the performance of pumps that had different operating (or construction) parameters than those seen up to now. In this cases we had not experimental measures of the pumping speed, but only the ratio between current and pressure. In particular we compared our simulations with pumps with different values of magnetic field, different voltage at cathodes, different anode rays. Generally speaking simulations gave good agreement with the experimental data, especially at low pressures. Some points in some curves turned out to be

incorrect, but although we still don't have a certain explanation, we think that they derive from cases in which the statistics of the distributions are not sufficient to calculate faithfully the current or that these distributions have been produced with a binning to be improved.
In conclusion our model seems to be able to simulate the performance of some sputter ion pumps actually on the market. Moreover, good results are generally given also for pumps with different constructive or operating parameters. However, at the moment these results are obtained by making some compromises:

- we can consider only $N_2$ as background gas, if we wanted to change we would have to implement the cross sections of the new gas and its other main characteristics (diffusion, generation of secondary ions, etc.);
- the approximations done for a single cell do not influence significantly the result if we consider pumps that have a low number of Penning cells; this is not true if we have a large number of Penning cells;
- the conductance calculation can be improved as in some cases it is a source of systematic errors;
- we do not have an exact calculation of the shape and volume of plasma;
- we have not really clear what happens at the plasma when we consider high magnetic field (higher than about 0.16 T);

All these points affect the accuracy of the simulation differently and future studies starting from this list may improve the quality of the simulation.

# Appendices

# OpenFoam configuration

Each step requires a series of files to be executed as shown in Fig.1.

OpenFOAM can not be used directly for the electromagnetic field simulation, but the solver of the tool can be easily modified in order to calculate it [6]. So at this point it is implemented the geometry of the single Penning cell in meshing tools. Given the symmetry of the problem it was sufficient to implement only a quarter of the cell in order to calculate the field.

To do this the file called *blockMeshDict* must be modified by inserting the geometric coordinates of the cell. The fundamental sections of this file are: *Foamfile, scale, vertices, blocks, edges, boundary, mergePatchPairs* (see Fig.2 and Fig.3).

The first section *FoamFile* is set by default and *scale* is equal to one in order to

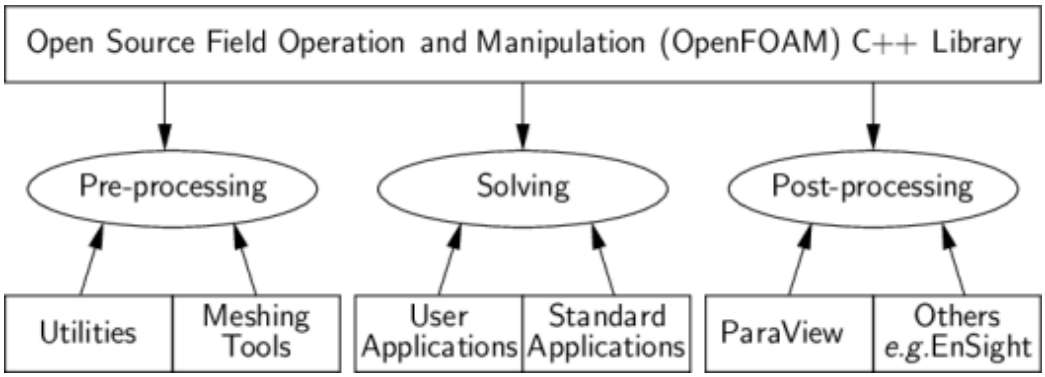


**Figure 1:** *An overview of OpenFOAM structure [34]*

```
/*--------------------------------*- C++ -*----------------------------------*\
  =========                 |
  \\      /  F ield         | OpenFOAM: The Open Source CFD Toolbox
   \\    /   O peration     | Website:  https://openfoam.org
    \\  /    A nd           | Version:  7
     \\/     M anipulation  |
\*---------------------------------------------------------------------------*/
FoamFile
{
    version     2.0;
    format      ascii;
    class       dictionary;
    object      blockMeshDict;
}
// * * * * * * * * * * * * * * * * * * * * * * * * * * * * * * * * * * * * //

scale 1;

vertices
(


    (x0 y0 z0)  //0
    (x1 y1 z1)  //1
    (x2 y2 z2)  //2
    .........
    (xn yn zn)  //n
);

blocks
(

    hex ( 0  1  13  0  3  4  14  3) (40 40 100) simpleGrading (  1 1 1)        //1 (mx2, my1, mz2)
    hex ( 0  13  2  0  3  14  5  3) (40 40 100) simpleGrading (  1 1 1)        //1 (mx2, my1, mz2)

    hex(.......................)(40 40 100) simpleGrading(  1 1 1)

);
```

**Figure 2:** *The first sections of blockMeshDict file*

have coordinates expressed in meters. In the *vertices* section the coordinates (x, y, z) of all the vertices of the portion of the cell are set expressed in meters. Each point has its own coordinates in round brackets. The order in which the points are written is important because each one corresponds to a number based on the position in which it is written. The section *blocks* contains all the three dimensional solids in which the figure is divided. For an easy geometry, as the Penning cell is, it is useful to divide it in hexahedral blocks. Each of these is defined by 8 vertices (written between round brackets) chosen from the list defined in the previous section. Then, for every block, are defined the number of cells in each direction and the cell expansion ratios after the command *simpleGrading*. The number of cells in each direction chosen is important because it determines the precision with which the fields will be calculated. But too high precision cannot be used as it would require a

```
edges
(
   //edges of anode
   arc 7 12 (x_edge_0 y_edge_0 z_edge_0)
   arc 12 8 (x_edge_1 y_edge_1 z_edge_1)

   arc k p (x_edge_n y_edge_n z_edge_n)

);

boundary
(

    symmetry-x
    {
        type symmetryPlane;
        faces
        (
            ( 0 1 4 3)
            ( 6 7 1 0)
            ( 3 4 10 9)
        );
    }
    symmetry-y
    {
        type symmetryPlane;
        faces
        (
            ( 0 2 5 3)
            ( 6 8 2 0)
            ( 3 5 11 9)
        );
    }

    ......................

);

mergePatchPairs
(
);
```

**Figure 3:** *The last sections of blockMeshDict file*

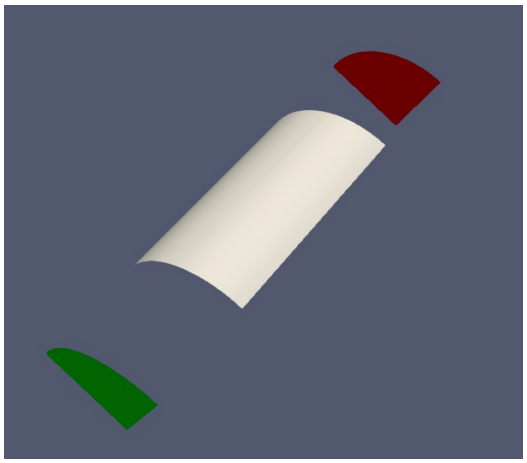

**Figure 4:** *A quarter cell penning implemented in openFOAM: in red and green are implemented the two cathodes and in white the anode*

lot of computing power. In section *edges* are defined the types of lines that link the vertices. For the case of the Penning cell are defined the arcs of circumference that connect the vertices. Between the brackets are written the coordinates of an intermediate point between the vertices intersected by the arc. After that in *boundary* are defined the roles of the faces that make up the geometry. For example in Fig.3 are defined the faces which define the planes of symmetry in the x and y directions. Other types of boundaries can be defined as explained in [34]. The command *mergePatchPairs* allows to define a mesh composed by more blocks. But in this case it is not necessary. The geometry implemented is reported in Fig.4

At this point the electric field and the potential are calculated inside the portion of space delimited by this geometry. This is done by managing the file *controlDict* as shown in Fig.5.

The command *application* allows to the user to set the solver; for this case the electrostatic solver is used. OpenFOAM is not able to solve static problems (like the one considered), but it is able to solve them considering their

```
FoamFile
{
    version     2.0;
    format      ascii;
    class       dictionary;
    location    "system";
    object      controlDict;
}
// * * * * * * * * * * * * * * * * * * * * * * * * * * * * * * * * * * * * * * * * * * * * //

application     electrostaticFoam;

startFrom       startTime;

startTime       0;

stopAt          endTime;

endTime         0.02;

deltaT          5e-5;

writeControl    timeStep;

writeInterval   100;

purgeWrite      0;

writeFormat     ascii;

writePrecision  6;

writeCompression off;

timeFormat      general;

timePrecision   6;

runTimeModifiable true;
```

**Figure 5:** *Control file to manage the solver options*

temporal evolution: that is why a start and end time must be set. Since the case in question is static, a very short simulation time is chosen. In the end, before proceeding a last file called *phi* must be modified by inserting the voltage values on the cathode and anode and how the field changes with respect to the other faces defined in *blockMeshDict* as shown in Fig.6.

In that file the dimensions of the physical quantities being considered are set. In particular the position of the numbers in brackets is relative to certain quantities (see Tab.1), while their value indicates the exponent to which these quantities should be raised.

```
dimensions      [1 2 -3 0 0 -1 0];

internalField   uniform 0;

boundaryField
{

    symmetry-x
    {
        type            symmetryPlane;
    }

    symmetry-y
    {
        type            symmetryPlane;
    }

    anode
    {
        type            fixedValue;
        value           uniform 0;
    }

    cathode-up
    {
        type            fixedValue;
        value           uniform -3000;
    }

    cathode-down
    {
        type            fixedValue;
        value           uniform -3000;
    }

    airDown-anode
    {
        type            zeroGradient;
    }
```

**Figure 6:** *The phi file where the boundary conditions of the problem are defined*

| Position | Property | SI unit |
|---|---|---|
| 1 | Mass | kilogram (kg) |
| 2 | Length | meter (m) |
| 3 | Time | second (s) |
| 4 | Temperature | Kelvin (K) |
| 5 | Quantity | mole (mol) |
| 6 | Current | ampere (A) |
| 7 | Luminosity intensity | candela (cd) |

**Table 1:** *The dimensions considered from openFOAM to define the field to simulate*

So in Fig.6 the dimensions considered are $kg \cdot m^2 \cdot s^{-3} \cdot A^{-1}$ which are *volts*. With the parameter *internalField* is set the initial condition at the beginning of the simulation: in this case no field is considered at the beginning. Then the boundary conditions are set for the faces previously defined. In the example there are:

- two blocks called *symmetry-x* and *symmetry-y* that are defined as symmetry planes: so the solver does not assign to them a specific value;
- the blocks composed by *anode, cathode-up, cathode-down* where specific values are assigned (expressed in volts as set with the command *dimensions*);
- the block *airDown-anode* that fixes the volume with a zero-gradient field.

# List of Figures

# Bibliography


[1] A. Gast A. Adamson. *Physical Chemistry of surfaces*. 1997.

[2] A.D. Appelhans and D.A. Dahl. "Measurement of external ion injection and trapping efficiency in the ion trap mass spectrometer and comparison with a predictive model". In: *International Journal of Mass Spectrometry* 216.3 (2002), pp. 269–284. ISSN: 1387-3806. DOI: https://doi.org/10.1016/S1387-3806(02)00627-9.

[3] M Audi and M de Simon. "Ion pumps". In: *Vacuum* 37.8 (1987). Special Issue Modern Vacuum Practice, pp. 629–636. ISSN: 0042-207X. DOI: https://doi.org/10.1016/0042-207X(87)90048-0.

[4] Rene Brun and Fons Rademakers. "ROOT - An Object Oriented Data Analysis Framework". In: *Proceedings AIHENP'96 Workshop, Lausanne, Sep. 1996,Nucl. Inst. and Meth. in Phys. Res. A 389 (1997) 81-86.* (). DOI: 10.5281/zenodo.3895860.

[5] T. B. Mitchell C. Barnes and M. M. Schauer. "Beyond the Brillouin limit with the Penning Fusion Experiment". In: *AIP Publishing* (). DOI: http://dx.doi.org/10.1063/1.872276.

[6] *CAELinux*. http://www.caelinux.com.

[7] Carraro Carlo. “Progettazione e tests del sistema di cattura e rivelazione per l’esperimento ATHENA”. PhD thesis. Università degli Studi di Genova, 2000.

[8] P. Clausing. “The Flow of Highly Rarefied Gases through Tubes of Arbitrary Length”. In: *Journal of Vacuum Science and Technology* 8.5 (1971), pp. 636–646. DOI: 10.1116/1.1316379.

[9] Hans Dehmelt. “Stored-Ion Spectroscopy”. In: (Jan. 1983). DOI: 10.1007/978-1-4613-3715-7_6.

[10] J.R. Dormand and P.J. Prince. “A family of embedded Runge-Kutta formulae”. In: *Journal of Computational and Applied Mathematics* 6.1 (1980), pp. 19–26. ISSN: 0377-0427. DOI: https://doi.org/10.1016/0771-050X(80)90013-3.

[11] Daniel H. E. Dubin and T. M. O’Neil. “Trapped nonneutral plasmas, liquids, and crystals (the thermal equilibrium states)”. In: *Rev. Mod. Phys.* 71 (1999), pp. 87–172. DOI: 10.1103/RevModPhys.71.87. URL: https://link.aps.org/doi/10.1103/RevModPhys.71.87.

[12] S. Gorp et al. “Simbuca, using a graphics card to simulate Coulomb interactions in a penning trap”. In: *Nuclear Instruments and Methods in Physics Research Section A: Accelerators, Spectrometers, Detectors and Associated Equipment* 638 (May 2011), pp. 192–200. DOI: 10.1016/j.nima.2010.11.032.

[13] Roy W. Gould. “Dynamics of non-neutral plasmas”. In: *Physics of Plasmas* 2.6 (1995), pp. 2151–2163. DOI: 10.1063/1.871302.

[14] Taekyun Ha and Sukmin Chung. “Optimization of cell geometry for a conventional sputter ion pump by a particle-in-cell simulation”. In: *Journal of Vacuum Science and Technology A* (2009). DOI: https://doi.org/10.1116/1.3106632.

[15] Marsbed Hablanian. “Chapter 2.1 - Technology of Vacuum Pumps—An Overview”. In: *Handbook of Vacuum Science and Technology*. Ed. by Dorothy M. Hoffman et al. San Diego: Academic Press, 1998, pp. 59–83. ISBN: 978-0-12-352065-4. DOI: https://doi.org/10.1016/B978-012352065-4/50051-1.

[16] L Hargreaves et al. “Differential cross sections for excitation of H2 by low-energy electron impact”. In: *Journal of Physics B: Atomic, Molecular and Optical Physics* 50 (Nov. 2017). DOI: 10.1088/1361-6455/aa9048.

[17] D. J. Harra. “Review of sticking coefficients and sorption capacities of gases on titanium films”. In: *Journal of Vacuum Science and Technology* 13.1 (1976), pp. 471–474. DOI: 10.1116/1.568900.

[18] H. Hartwig and J. S. Kouptsidis. “A new approach for computing diode sputter-ion pump characteristics”. In: *Journal of Vacuum Science and Technology* 11.6 (1974), pp. 1154–1159. DOI: 10.1116/1.1318701.

[19] J. C. Helmer and R. L. Jepsen. “Electrical Characteristics of a Penning Discharge”. In: *Proceedings of the IRE* 49.12 (1961), pp. 1920–1925. DOI: 10.1109/JRPROC.1961.287721.

[20] “Chapter 1.8 - Surface Physics and Its Relation to Vacuum Science”. In: *Handbook of Vacuum Science and Technology*. Ed. by Dorothy M. Hoffman et al. San Diego: Academic Press, 1998, pp. 40–55. ISBN: 978-

0-12-352065-4. DOI: https://doi.org/10.1016/B978-012352065-4/50050-X.

[21] Yukikazu Itikawa. "Cross Sections for Electron Collisions with Nitrogen Molecules". In: *Journal of Physical and Chemical Reference Data* 35.1 (2006), pp. 31–53. DOI: 10.1063/1.1937426.

[22] Ashok Jain and K. L. Baluja. "Total (elastic plus inelastic) cross sections for electron scattering from diatomic and polyatomic molecules at 10–5000 eV: $H_2$, $Li_2$, HF, $CH_4$, $N_2$, CO, $C_2H_2$, HCN, $O_2$, HCl, $H_2S$, $PH_3$, $SiH_4$, and $CO_2$". In: *Phys. Rev. A* 45 (1 1992), pp. 202–218. DOI: 10.1103/PhysRevA.45.202.

[23] R. L. Jepsen. "Magnetically Confined Cold-Cathode Gas Discharges at Low Pressures". In: *Journal of Applied Physics* 32.12 (1961), pp. 2619–2626. DOI: 10.1063/1.1728362.

[24] M. A. Khakoo and S. Trajmar. "Elastic electron scattering cross sections for molecular hydrogen". In: *Phys. Rev. A* 34 (1 1986), pp. 138–145. DOI: 10.1103/PhysRevA.34.138.

[25] W. Knauer. "Mechanism of the Penning Discharge at Low Pressures". In: *Journal of Applied Physics* 33.6 (1962), pp. 2093–2099. DOI: 10.1063/1.1728902.

[26] Martina Knoop, Niels Madsen, and Richard C Thompson. *Trapped Charged Particles*. WORLD SCIENTIFIC (EUROPE), 2016. DOI: 10.1142/q0004.

[27] Martin Knudsen. "Die Gesetze der Molekularströmung und der inneren Reibungsströmung der Gase durch Röhren". In: *Annalen der Physik* 333.1 (1909), pp. 75–130. DOI: https://doi.org/10.1002/andp.19093330106.

[28] E.M. Lifshitz L.D. Landau. *Statistical Physics*. Vol. 5. 1980. DOI: https://doi.org/10.1016/C2009-0-24487-4.

[29] P.J. Linstrom and W.G. Mallard. "NIST Chemistry WebBook, NIST Standard Reference Database Number 69". In: DOI: https://doi.org/10.18434/T4D303.

[30] N. Matsunami et al. "A semiempirical formula for the energy dependence of the sputtering yield". In: *Radiation Effects* 57.1-2 (1981), pp. 15–21. DOI: 10.1080/01422448008218676.

[31] B. L. Moiseiwitsch, A. Williams, and David Robert Bates. "The elastic scattering of fast electrons and positrons by hydrogen and helium atoms". In: *Proceedings of the Royal Society of London. Series A. Mathematical and Physical Sciences* 250.1262 (1959), pp. 337–345. DOI: 10.1098/rspa.1959.0067.

[32] R.S. Myong. "Gaseous slip models based on the Langmuir adsorption isotherm". In: *Physics of fluids* 16.1 (2004). DOI: 10.1063/1.1630799.

[33] C.B. Opal, E.C. Beaty, and W.K. Peterson. "Tables of secondary-electron-production cross sections". In: *Atomic Data and Nuclear Data Tables* 4 (1972), pp. 209–253. ISSN: 0092-640X. DOI: https://doi.org/10.1016/S0092-640X(72)80004-4.

[34] *OpenFOAM*. https://www.openfoam.com/documentation/user-guide/.

[35] T. M. O'Neil. "Plasmas with a single sign of charge". In: *AIP Conference Proceedings* 175.1 (1988), pp. 1–7. DOI: 10.1063/1.37619.

[36] Chiara Paolini, Mauro Audi, and Mark Denning. "Ion Pump Design for Improved Pumping Speed at Low Pressure". In: *Applied Science and Convergence Technology* 25 (Nov. 2016), pp. 108–115. DOI: 10.5757/ASCT.2016.25.6.108.

[37] Chiggiato Paolo. "Vacuum Technology for Ion Sources". In: *CAS-CERN Accelerator School: Ion Sources - Proceedings* (Apr. 2014). DOI: 10.5170/CERN-2013-007.463.

[38] S. A. Prasad and T. M. O'Neil. "Finite length thermal equilibria of a pure electron plasma column". In: *The Physics of Fluids* 22.2 (1979), pp. 278–281. DOI: 10.1063/1.862578.

[39] W. H. et al. Press. "Numerical Recipes: The Art of Scientific Computing". In: 2007, pp. 910–920.

[40] Donald J. Santeler. "New concepts in molecular gas flow". In: *Journal of Vacuum Science & Technology A* 4.3 (1986), pp. 338–343. DOI: 10.1116/1.573923.

[41] . 2020. URL: http://cds.cern.ch/record/2646487.

[42] *Ion getter pumps*. 2020. URL: http://cds.cern.ch/record/2646487.

[43] W. Schuurman. “Investigation of a low pressure penning discharge”. In: *Physica* 36.1 (Jan. 1967), pp. 136–160. DOI: 10.1016/0031-8914(67)90086-9.

[44] Lawrence F. Shampine. “Some Practical Runge-Kutta Formulas”. In: *Mathematics of Computation* 46.173 (1986), pp. 135–150.

[45] T. W. Shyn, W. E. Sharp, and Y.-K. Kim. “Doubly differential cross sections of secondary electrons ejected from gases by electron impact: 25-250 eV on $H_2$”. In: *Phys. Rev. A* 24 (1 1981), pp. 79–88. DOI: 10.1103/PhysRevA.24.79.

[46] *Simbuca on SourceForge*. http://sourceforge.net/projects/Simbuca/.

[47] J. H. Singleton. “Hydrogen Pumping by Sputter-Ion Pumps and Getter Pumps”. In: *Journal of Vacuum Science and Technology* 8.1 (1971), pp. 275–282. DOI: 10.1116/1.1316309.

[48] Sven Sturm et al. “Investigation of Space-Charge Phenomena in Gas-Filled Penning Traps”. In: *AIP Conference Proceedings* 1114.1 (2009), pp. 185–190. DOI: 10.1063/1.3122282.

[49] Dylan J. Temples. *Elementary Particle Physics in a Nutshell - M. Tully*. 2017.

[50] “The Penning Trap”. In: *Charged Particle Traps: Physics and Techniques of Charged Particle Field Confinement*. Berlin, Heidelberg: Springer Berlin Heidelberg, 2005, pp. 51–85. ISBN: 978-3-540-26576-4. DOI: 10.1007/3-540-26576-7_3. URL: https://doi.org/10.1007/3-540-26576-7_3.

[51] Richard C. Thompson. *Trapped Charged Particles*. DOI: https://doi.org/10.1142/q0004.

[52] Loup Verlet. "Molecular Dynamics: Computer 'Experiments' on Simple Liquids". In: Jan. 1974, pp. 469–478. ISBN: 978-94-010-2179-1. DOI: 10.1007/978-94-010-2177-7_45.

[53] Y X Wang and J M Wen. "Gear Method for Solving Differential Equations of Gear Systems". In: *Journal of Physics: Conference Series* 48 (2006), pp. 143–148. DOI: 10.1088/1742-6596/48/1/026.

[54] H.G. Weller et al. "A Tensorial Approach to Computational Continuum Mechanics Using Object Orientated Techniques". In: *Computers in Physics* 12 (Nov. 1998), pp. 620–631. DOI: 10.1063/1.168744.